Identification of (Z)-2-benzylidene-dihydroimidazothiazolone derivatives as tyrosinase inhibitors: Anti-melanogenic effects and *in silico* studies

Heejeong Choi [a,1], Il Young Ryu [a,1], Inkyu Choi [a,1], Sultan Ullah [b,1], Hee Jin Jung [a,1], Yujin Park [a], YeJi Hwang [a], Yeongmu Jeong [a], Sojeong Hong [a], Pusoon Chun [c], Hae Young Chung [a], Hyung Ryong Moon [a,*]

[a] *College of Pharmacy, Pusan National University, Busan 46241, South Korea*
[b] *Department of Molecular Medicine, The Scripps Research Institute, FL 33458, USA*
[c] *College of Pharmacy and Inje Institute of Pharmaceutical Sciences and Research, Inje University, Gimhae, Gyeongnam 50834, South Korea*

ARTICLE INFO

ABSTRACT

As part of our continuous search for novel tyrosinase inhibitors, we designed 5,6-dihydroimindazo[2,1-*b*]thiazol-3(2*H*)-one (DHIT) derivatives based on the structure of MHY773; a potent tyrosinase inhibitor with a 2-iminothiazolidin-4-one template. Of the 11 DHIT derivatives synthesized using a Knoevenagel condensation, three DHIT derivatives **1a** (IC_{50} = 36.14 ± 3.90 μM), **1b** (IC_{50} = 0.88 ± 0.91 μM), and **1f** (IC_{50} = 17.10 ± 1.01 μM) inhibited mushroom tyrosinase more than kojic acid (IC_{50} = 84.41 ± 2.87 μM). Notably, compound **1b** inhibited mushroom tyrosinase around 100- and 3.3-fold more potently than kojic acid and MHY773, respectively. Lineweaver-Burk plots demonstrated that compounds **1b** and **1f** competitively inhibited mushroom tyrosinase, and *in silico* docking results supported our kinetic results and indicated that these two compounds bind more strongly to the active site of tyrosinase than kojic acid. Docking simulation results using a human tyrosinase homology model confirmed the abilities of **1b** and **1f** to strongly inhibit human tyrosinase. B16F10 murine melanoma cells were used to investigate whether these two compounds display tyrosinase inhibitory activities and anti-melanogenesis effects in cells. Both compounds were found to significantly and dose-dependently inhibit cellular tyrosinase activity and intracellular and extracellular melanin production more potently than kojic acid. The similarities observed between the cellular tyrosinase and melanogenesis inhibitory effects of **1b** and **1f** suggest their observed anti-melanogenic effects were due to tyrosinase inhibition. These results indicate that compounds **1b** and **1f**, which possess the DHIT template, are promising candidates as anti-browning agents and therapeutic agents for hyperpigmentation disorders.

© 2022 The Authors. Published by Elsevier B.V. on behalf of Research Network of Computational and Structural Biotechnology. This is an open access article under the CC BY license (http://creativecommons.org/licenses/by/4.0/).

1. Introduction

Tyrosinase (TYR, EC 1.14.18.1) is the rate-limiting enzyme in melanogenesis and is found in mammals, plants, fungi, and bacteria. Human tyrosinase (*h*TYR), which belongs to the mammalian tyrosinase family, is a type 3 copper-containing metalloenzyme and a glycoprotein comprised of 529 amino acids. At its active site, two magnetically bound copper ions (Cu_a and Cu_b) are linked by a hydroxo ligand in the *met* state and coordinated with six histidine residues [1]. The primary function of *h*TYR is to oxidize L-tyrosine to L-DOPA by acting as monophenolase and subsequently to convert L-DOPA to dopaquinone by acting as a diphenolase [2]. This double oxidation process leads to the formation of melanin. Two other enzymes, tyrosinase-related proteins 1 and 2 (*h*TYRP1 and *h*TYRP2) are also known to participate in the production of melanin. The final products of melanogenesis are eumelanin (a dark brown to black pigment) and pheomelanin (a yellow/red pigment) [3]. Melanogenesis occurs in melanocytes, a specialized type of dendritic cell, located in skin, hair bulbs, and eyes. At the subcellular level, melanins are stored in melanosomes and importantly protect skin against UV radiation and free radicals. However, abnormal productions of melanins can cause pathological

conditions, which include melasma, lentigo, congenital melanocytic naevi, erythormelanosis follicularis faciei et colli, post-inflammatory hyperpigmentation, and erythema dyschromicum perstans [4]. Because *h*TYR catalyzes the first two steps of melanogenesis, most of the efforts made to suppress or reduce melanin production have been directed at the development of effective TYR inhibitors. This strategy has proven to be effective and a strong correlation has been demonstrated between TYR inhibition and levels of melanin generated [5]. Thus, *h*TYR is considered an attractive target for reducing melanogenesis but is rarely used due to the high price of *h*TYR and the difficulties associated with their productions in stable forms [5]. To assay TYR inhibitory activity of potential tyrosinase inhibitors, mushroom (*Agaricus bisporus*) tyrosinase (*ab*TYR) is widely used as a study model because of its availability, low cost and reliable results.

Thousands of TYR inhibitors have been reported [6-11], and some, such as kojic acid [12], hydroquinone, monobenzyl hydroquinone, arbutin [13-17], salicylhydroxamic acid [18], azelaic acid [19], rucinol [20], phenylethyl resorcinol [21], thiazolyl resorcinols [22], and corticosteroids [18,19], exhibit excellent anti-melanogenic effects in cell-based assays [23-35]. However, many of these inhibitors have been reported to have severe side effects, such as skin cancer, irreversible depigmentation, and dermatitis, in animal and human models [36]. Hydroquinone and kojic acid are banned in most countries due to their carcinogenic [37], nephrotoxic [38], melanocytoxic [39], and genotoxic [40] effects. Arbutin (a natural tyrosinase inhibitor) has lesser side effects but has stability issues, for example, it is hydrolyzed to hydroquinone and D-glucose by thermodegradation at 20 °C and skin microflora [41,42] Accordingly, research efforts are aimed at identifying safer, more potent stable tyrosinase inhibitors.

During our studies on this topic over past decades, we have identified a number of benzylidene derivatives with the β-phenyl-α,β-unsaturated carbonyl scaffold more potently inhibit tyrosinase than kojic acid, a representative tyrosinase inhibitor (Fig. 1) [29,43-66].

Celecoxib and rofecoxib are nonsteroidal anti-inflammatory drugs. Although rofecoxib was withdrawn from the market due to increased heart attack risk, rofecoxib with a higher log P value penetrated the blood–brain barrier better than celecoxib. As such, log P values are closely related to brain penetration of drugs and absorption of drugs into the skin and gastrointestinal tract. Previously, we synthesized (Z)-5-(3-hydroxy-4-methoxybenzylidene)-2-iminothiazolidin-4-one (MHY773, Fig. 1), which possesses a 2-iminothiazolidin-4-one template, and found this compound potently inhibited mushroom tyrosinase (IC$_{50}$ = 2.87 μM for monophenolase and 8.06 μM for diphenolase) and melanogenesis in B16F10 melanoma cells [56]. The effectiveness of whitening agents depend on how well they access melanocytes in the epidermal basal layer, and skin permeability is known to be closely related to lipophilicity. As shown in Fig. 2, the chemical structure of 5,6-dihydroimidazo[2,1-*b*]thiazol-3(2*H*)-one (DHIT) is similar to that of 2-iminothiazolidin-4-one, which is more lipophilic, and thus, we expected derivatives with the DHIT template to potently inhibit tyrosinase and melanin production. Thus, we selected as a novel core template for tyrosinase inhibitors and designed and synthesized 11 DHIT derivatives with a 2-benzylidene group bearing a variety of substituents. These 11 derivatives were evaluated for mushroom tyrosinase inhibitory activity at the enzyme level and for tyrosinase activity and melanogenesis in cell-based systems. The underlying mechanisms involved were investigated using Lineweaver-Burk double reciprocal plots, and to investigate the possibility that these derivatives inhibit human tyrosinase, a homologous model for human tyrosinase was prepared and docking simulations were performed.

2. Results and discussion

2.1. Chemistry

First, 5,6-dihydroimidazo[2,1-*b*]thiazol-3(2*H*)-one (**2**) [67], the DHIT template, was prepared by reacting 2-thioimidazolidine with ethyl chloroacetate in the presence of sodium acetate (yield 72%) (Scheme 1) [68]. Reaction of **2** with benzaldehydes under Knoevenagel condensation conditions using sodium acetate/acetic acid gave benzylidene derivatives **1a** – **1 k** (all bearing the DHIT template) in yields of 37 to 88% [69]. To examine the effects of substituents of the benzylidene moiety on tyrosinase inhibition, various benzaldehydes bearing substituents such as a hydroxyl, a methoxyl, and/or an ethoxyl group were condensed with **2**. A total of 11 derivatives with the DHIT template were synthesized.

The structures of the eleven DHIT derivatives were determined by ^{1}H and ^{13}C NMR and mass (MS) spectroscopy. The double bond geometries of all 11 derivatives (**1a** – **1 k**) were assigned to the (*Z*)-configuration based on vicinal ^{1}H, ^{13}C-coupling constants (^3J) in proton-coupled ^{13}C NMR spectra. According to a report by Nair et al. [70], different vicinal ^{1}H, ^{13}C-coupling constants in proton-coupled ^{13}C NMR spectra are observed for geometric isomers of a variety of trisubstituted α ,β-unsaturated carbonyl compounds, including 5-membered and 6-membered exocyclic methylene carbonyl compounds. As depicted in Fig. 3, vicinal coupling constants between the amide carbonyl C-atom C(1) and the olefinic H-atom at C(3) in proton-coupled ^{13}C NMR spectra depended on double bond stereochemistry: (*Z*)-isomer: $^3J_{trans}$ = 11.5 Hz, and (*E*)-isomer: $^3J_{cis}$ = 6.8 Hz. Generally, $^3J_{cis}$ values range from 3.6 to 7.0 Hz, while the range of $^3J_{trans}$ is roughly twice as large (typically ≥ 10 Hz) [71]. For compound **I** (Fig. 3), the amide carbonyl carbon had a vicinal ^{1}H, ^{13}C-coupling constant of 6.3 Hz ($^3J_{(C(3), H-C(1))}$) [71]. The ^{13}C NMR of compound **1b** was measured in proton-coupled ^{13}C mode, and the ^3J value of C3 in **1j** was 6.0 Hz (Fig. S30 in Supplementary data), suggesting a (*Z*)-configuration.

2.2. Tyrosinase inhibition - Kinetics, mechanism, and in silico and in vitro studies

2.2.1. Mushroom tyrosinase inhibition

The anti-tyrosinase efficacies of the 11 synthesized DHIT derivatives **1a** – **1 k** against mushroom tyrosinase (*m*TYR) were investigated as we previously described for the evaluation of *m*TYR inhibitory activity [65]. Table 1 summarizes % inhibition results for **1a** – **1 k** at a concentration of 25 μM. Kojic acid was used as a positive control, as is typical for tyrosinase inhibitor evaluations. Compounds **1 g**, **1 h**, **1i**, and **1 k** with no hydroxyl substituent showed low or no *m*TYR inhibitory activity, whereas compounds **1a**, **1b**, and **1f** inhibited *m*TYR more than kojic acid (30% inhibition) at 25 μM. Compound **1a** (40% inhibition) with a 4-hydroxyl substituent on the phenyl ring inhibited *m*TYR slightly more than kojic acid. However, compound **1f** (73% inhibition) with a 3-hydroxy-4-methoxyl substituent on the phenyl ring inhibited *m*TYR more than compound **1a**. Compound **1b** (96% inhibition) with a hydroxyl at the 2- and 4-positions of the phenyl ring had greatest inhibitory effect. Considering the potent *m*TYR inhibitory activities of compounds **1a** and **1b**, it seemed that the presence of a 4-hydroxyl on the phenyl ring markedly increased *m*TYR inhibition, but compounds **1d** and **1e**, which also possessed a 4-hydroxyl exhibited only low mushroom tyrosinase inhibitory activity (7 and 3%, respectively). These results indicate that the presence of a 4-hydroxyl on the phenyl rings of DHIT derivatives can markedly influence *m*TYR inhibition, but that the additional presence of a 3-alkoxyl (3-methoxyl in **1d**, or 3-ethoxyl in **1e**) substituent or a
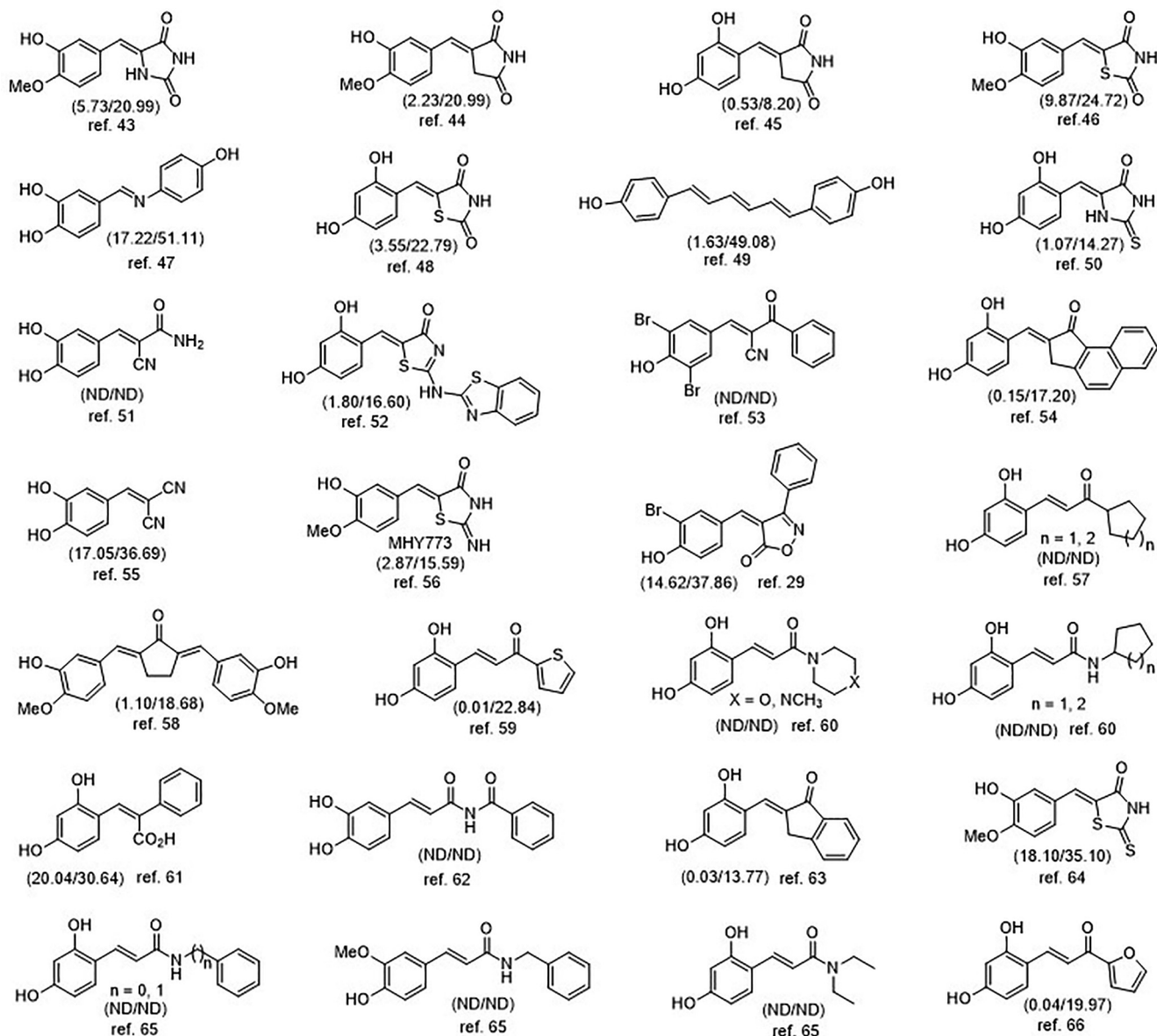
Fig. 1. Substituted benzylidene tyrosinase inhibitors with a variety of templates. The values in parenthesis represent IC_{50} values (µM) of the corresponding compound and kojic acid, respectively. ND means 'not determined'.
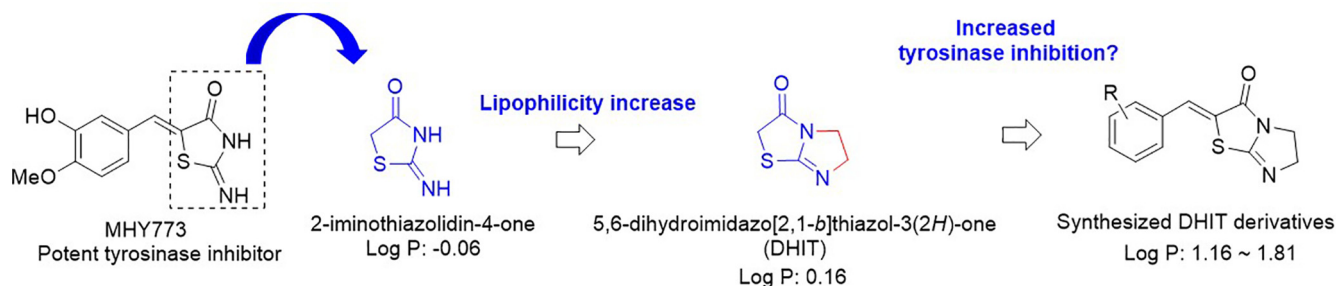

Fig. 2. Rationale for the design of DHIT derivatives.

3,5-dialkoxyl (3,5-dimethoxyl in **1j**) suppresses 4-hydroxyl-induced decreases in *m*TYR activity. Compounds **1b** and **1c** had a 4-hydroxyl substituent and at a different position on the phenyl ring had an extra hydroxyl substituent. Interestingly, these compounds inhibited *m*TYR to different extents, that is, compound **1b** inhibited *m*TYR by 96% whereas compound **1c** inhibited *m*TYR by only 18%. These results indicate that the position of an extra hydroxyl substituent on the 4-hydroxyphenyl ring can greatly influence
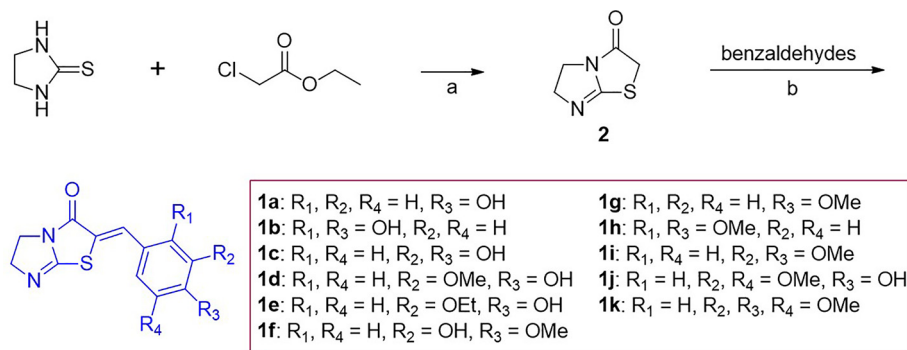
Scheme 1. Synthetic scheme for (*Z*)-2-(substituted benzylidene)-5,6-dihydroimidazo[2,1-*b*]thiazol-3(2*H*)-one derivatives. Reagents and conditions: (a) NaOAc, EtOH, reflux, 21 h, 72%; (b) NaOAc, acetic acid, 80 °C, 2 – 12 h, 37 – 88%.
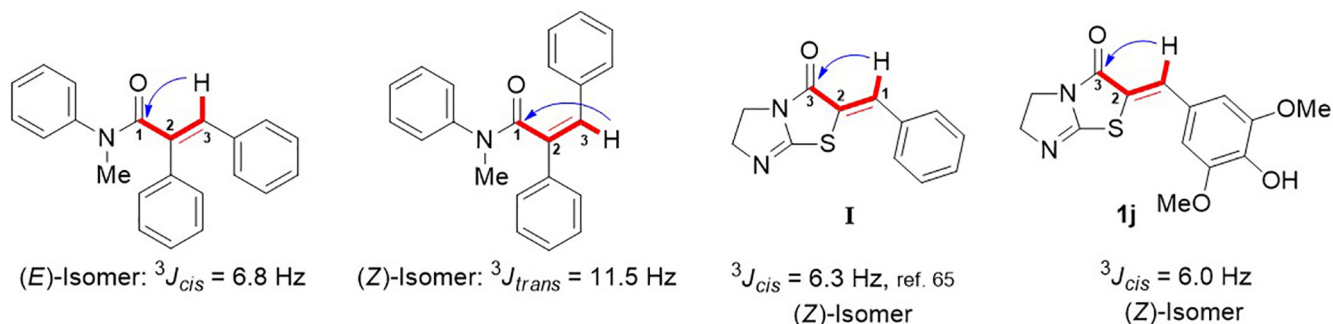

Fig. 3. Relationships between the geometry of the α -carbonyl C = C double bond and C,H-spin-coupling constants over three bonds as indicated by the arrow.

Table 1
Substitution patterns and mushroom tyrosinase inhibitions after treatment with (*Z*)-2-(substituted benzylidene)-5,6-dihydroimidazo[2,1-*b*]thiazol-3(2*H*)-one derivatives **1a** – **1 k** or kojic acid, and log P values.

1a - 1k

Compound	R₁	R₂	R₃	R₄	Tyrosinase inhibition (%)	IC₅₀ (µM)	Synthetic yield (%)	ᵃLog P
1a	H	H	OH	H	40.89 ± 0.68	36.14 ± 3.90	68	1.55
1b	OH	H	OH	H	96.69 ± 0.01	0.88 ± 0.91	59	1.16
1c	H	OH	OH	H	18.96 ± 0.44	>100	74	1.16
1d	H	OMe	OH	H	7.83 ± 2.29	>100	37	1.42
1e	H	OEt	OH	H	3.90 ± 2.65	>100	72	1.76
1f	H	OH	OMe	H	73.73 ± 1.35	17.10 ± 1.01	63	1.42
1 g	H	H	OMe	H	9.32 ± 1.08	>100	65	1.81
1 h	OMe	H	OMe	H	13.41 ± 0.93	>100	73	1.69
1i	H	OMe	OMe	H	ᵇNI	>100	88	1.69
1j	H	OMe	OH	OMe	24.43 ± 1.50	>100	55	1.30
1 k	H	OMe	OMe	OMe	NI	>100	78	1.56
ᶜKA					30.26 ± 0.55	84.41 ± 2.87		−2.45

Tyrosinase inhibition experiments were conducted using synthesized derivatives or kojic acid at a concentration of 25 µM. ᵃLog P values were obtained using ChemDraw Ultra 12.0. ᵇNI means no inhibition. ᶜKA means kojic acid.

*m*TYR inhibition. Our accumulated SAR data on tyrosinase inhibitors bearing a β -phenyl- α, β -unsaturated carbonyl motif also suggests that compounds with a 2,4-dihydroxyl or 3-hydroxy-4-methoxyl substituent on the β -phenyl ring potently inhibit *m*TYR (Fig. 1). In accord with our collated SAR results, compound **1b** with a β −2,4-dihydroxyphenyl group and compound **1f** with a β −3-hydroxy-4-methoxyphenyl group were found to most potently inhibit *m*TYR. According to the cumulative docking simulation results, the 2,4-dihydroxyl substituent on the β -phenyl ring contributes to strong binding to tyrosinase through hydrogen bonding

at the active site, implying that the 2,4-dihydroxyl substituent plays an important role in tyrosinase inhibition. In some compounds [53,58,61,62,64,66], both hydroxyl groups of the 2,4-dihydroxyl substituent participate in hydrogen bonding as hydrogen bond donors, and in some compounds [49,60,61,67] only one of the two hydroxyls participates in hydrogen bonding as a hydrogen bond donor.

Because DHIT derivatives potently inhibited mushroom tyrosinase, we investigated the IC_{50} values of the synthesized DHIT derivatives. The three active derivatives **1a**, **1b**, and **1f** dose-dependently inhibited *m*TYR (data not shown). The IC_{50} value of kojic acid, the positive control, was 84.41 μM, while those of DHIT derivatives **1a** and **1f** were 36.14 and 17.10 μM, respectively, indicating that they were 2.3- and 4.9-fold stronger tyrosinase inhibitors than kojic acid. Compound **1b** inhibited *m*TYR most with an IC_{50} value of 0.88 μM, which showed it inhibited *m*TYR 100-fold more than kojic acid. The other DHIT derivatives had IC_{50} values above 100 μM.

Log P values of the synthesized DHIT derivatives were obtained using ChemDraw Ultra 12.0. As indicated in Table 1, DHIT derivatives had log P values ranging from 1.16 to 1.81, which showed they were more lipophilic than the corresponding derivatives with the 2-iminothiazolidin-4-one template.

2.2.2. Determination of the inhibitory mechanism by enzyme kinetics

Since compounds **1b** and **1f** most potently inhibited *m*TYR, they were subjected to kinetic study. Lineweaver-Burk double reciprocal plots were used to determine their inhibitory modes of action. Kinetic analyses were carried out using four concentrations of DHIT derivatives **1b** (0, 0.0625, 0.125, or 0.25 μM) and **1f** (0, 1, 2, or 4 μM) in the presence of different concentrations of L-tyrosine (0.5, 1, 2, 4, 8, or 16 mM for **1b** and 1, 2, 4, or 8 mM for **1f**). Results are summarized in Fig. 4. Lineweaver-Burk double reciprocal plots produced four different lines with different slopes, corresponding to the four concentrations, for each derivative. In each case, the four different lines converged at one point on the y-axis, indicating that the V_{max} values of the two compounds (0.0126 mM/min for **1b** and 0.0103 mM/min for **1f**) were independent of concentration. In addition, the results showed that the K_M values of **1b** and **1f** increased in a concentration-dependent manner, which suggested that both bind to the same binding pocket as L-tyrosine and competitively inhibit *m*TYR. K_M values were 1.515, 7.846, 15.740, and 23.586 mM at 0, 0.0625, 0.125, and 0.25 mM of **1b**, and 3.758, 4.892, 5.206, and 8.127 mM at 0, 1, 2, and 4 μM of **1f**, respectively. Furthermore, the kinetic studies showed that K_i values were 1.50×10^{-8}, 1.33×10^{-8}, and 1.72×10^{-8} M at 0.0625, 0.125, 0.25 μM of **1b**, and 3.31×10^{-6}, 5.19×10^{-6}, and 3.44×10^{-6} M at 1, 2, and 4 μM of **1f**, respectively. The binding abilities of compounds **1b** and **1f** to the active site of tyrosinase were also supported by *in silico* docking simulation results (Figs. 5 and 6).

*2.2.3. In silico studies of compounds **1b** and **1f** using the crystal structure of mTYR and a hTYR homology model*

A docking study was performed using Schrodinger suite (release 2021–1) to further investigate the tyrosinase enzyme inhibitory effects of compounds **1b** and **1f**. Both compounds potently inhibited *m*TYR in the mushroom tyrosinase assay (Table 1), and kinetic studies confirmed the competitive nature of these inhibitions (Fig. 4). To determine whether **1b** and **1f** bind directly to the active sites of *m*TYR and *h*TYR, we docked compounds **1b** and **1f** to the crystal structure of *m*TYR and to a prepared human tyrosinase homology model, respectively, and compared the results with those obtained with kojic acid.

*2.2.3.1. Docking studies of derivatives **1b** or **1f** or kojic acid with mTYR.* The crystal structure of *m*TYR (*Agaricus bisporus* tyrosinase,

PDB ID: 2Y9X) was imported from the Protein Data Bank and docked against **1b**, **1f**, and kojic acid. Interactions between these three compounds and *m*TYR are shown in Fig. 5a in 2D and 3D. Docking results showed **1b** and **1f** occupied the same binding site as kojic acid. To further examine the natures of these interactions we considered pi-pi stacking, hydrophobic interactions, hydrogen bonding, and metal coordination. Kojic acid formed one hydrogen bond with the amino acid residue Met280 using the 5-hydroxyl group of its 4-pyrone ring at a distance of 2.20 Å. In addition, the 2-hydroxymethyl group of its 4-pyrone ring coordinated with Cu401 at a distance of 2.36 Å, and the 4-pyrone ring interacted with His263 by pi-pi stacking, and also with Val283 hydrophobically. Based on these interactions, the recorded docking score for kojic acid was − 4.4 kcal/mol. Interestingly, the binding interactions between *m*TYR and **1b** and kojic acid were closely related. Like kojic acid, the 4-hydroxyl group of the phenyl ring of **1b** also coordinated with Cu401, although notably, the 4-hydroxyl group of the phenyl ring of **1b** also coordinated with Cu400 and formed salt bridges with Cu400 and Cu401 at distances of 2.28 and 2.32 Å, respectively. However, unlike kojic acid, **1b** did not form hydrogen bonds though it did form two pi-pi stacking interactions with His259 and His263. In addition, **1b** interacted hydrophobically with Phe264, Met280, and Val283. Due to these interactions, **1b** had a docking score of − 6.7 kcal/mol, that is, docking analysis indicated it binds to the active site of tyrosinase much more strongly than kojic acid. The 3D structures in Fig. 5 also show that in its bound position **1b** is located closer to the two copper ions than kojic acid. On the other hand, **1f**, unlike kojic acid and **1b**, did not coordinate with copper ions or form a salt bridge, and made one hydrogen bond with Asn260 using the 3-hydroxyl group on its phenyl ring. Interestingly, **1f** interacted hydrophilically with His85, Hie244 (a protonated histidine form), His259, Asn260, and His263, and achieved a docking score of − 4.6 kcal/mol, that is, a score intermediates between those of kojic acid and compound **1b**. These results, which are in line with our kinetic study results, suggest that the strong *m*TYR inhibitory activities of **1b** and **1f** are due to strong binding with the active site of *m*TYR.

We also performed docking studies on the (*E*)-isomers of compounds **1b** and **1f** to determine whether the geometry of the compounds plays a role in the protein-binding interactions at the active site of tyrosinase, as shown in Fig. 5b. Surprisingly, both compounds still occupied the active site of the tyrosinase enzyme, but showed lower docking scores compared to the (*Z*)-isomers, **1b** and **1f**. The lower docking score of the (*E*)-isomer of **1b** may be due to the loss of salt bridges with copper ions. Also, the (*E*)-isomer of compound **1f** showed reverse conformation to that of the (*Z*)-isomer in the active site of tyrosinase enzyme. These docking results suggest that only the (*Z*)-isomers of **1b** and **1f** strongly inhibit the activity of the tyrosinase enzyme.

*2.2.3.2. Docking studies of derivatives **1b** or **1f** or kojic acid with a hTYR homology model.* After confirming direct binding between **1b** or **1f** and *m*TYR we performed docking simulations using a *h*TYR homology model. The model was based on human tyrosinase-related protein 1 (*h*TRP1, PDB: 5M8Q) which shares 45.81% sequence identity with *h*TYR (Fig. S37 in Supplementary data). Binding interactions between **1b**, **1f**, or kojic and the *h*TYR homology model are shown in Fig. 6a in 2D and 3D.

As shown by the 3D structure, the 2-hydroxymethyl group on the 4-pyrone ring of kojic acid coordinates with the two zinc ions (Zn6 and Zn7) at distances of 2.16 and 2.21 Å, respectively. Kojic acid also forms a hydrogen bond with Asn364 using the 5-hydroxyl group of its 4-pyrone ring and interacts by pi-pi stacking with His367 with a docking score of − 4.9 kcal/mol. This means that the binding affinity of kojic acid for the *h*TYR homology model was similar to that for *m*TYR.
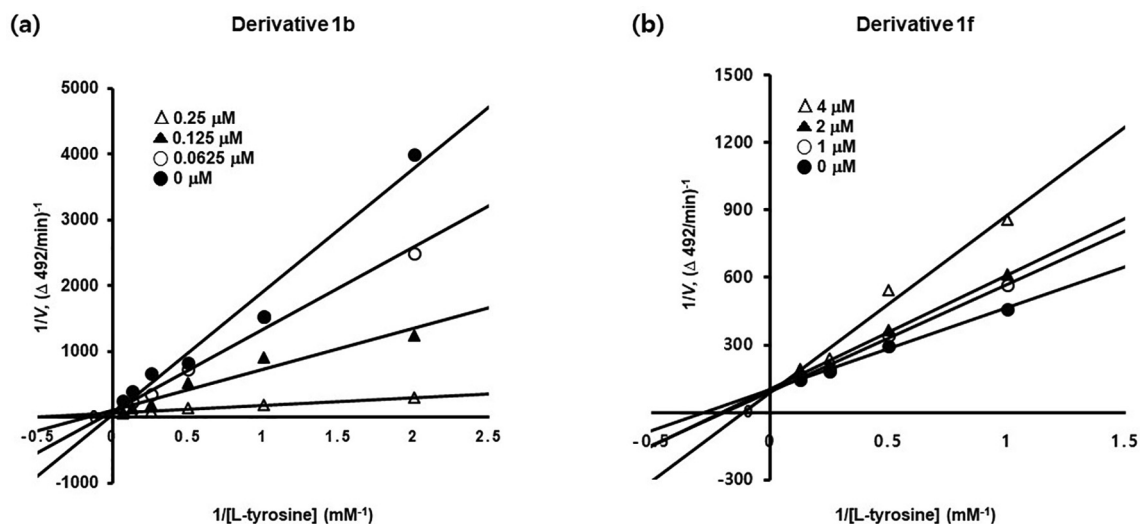
Fig. 4. Enzyme inhibition kinetic studies of DHIT derivatives **1b** (a) and **1f** (b) against mushroom tyrosinase. Lineweaver-Burk plots for the inhibition of mTYR were obtained at different concentrations of **1b** and **1f** (0 μM (closed circle), 0.0625 μM (open circle), 0.125 μM (closed triangle) and 0.25 μM (open triangle) for **1b**; and 0 μM (closed circle), 1 μM (open circle), 2 μM (closed triangle) and 4 μM (open triangle) for **1f**) in the presence of different concentrations of L-tyrosine (0.5, 1, 2, 4, 8, or 16 mM for **1b** and 1, 2, 4, or 8 mM for **1f**).

As regards compound **1b**, the 4-hydroxyl group on its phenyl ring coordinated and formed salt bridges with both zinc ions at distances of 2.16 and 2.20 Å, respectively, which were approximately the same as distances observed for kojic acid. Like kojic acid, the 2-hydroxyl group on the phenyl ring of **1b** formed a hydrogen bond with Met374 and interacted by pi-pi stacking with His363 and His367. Additionally, the 2-hydroxyl group on the phenyl ring and the DHIT carbonyl moiety of **1b** interacted hydrophobically with positively charged Lys306, Ser360, His363, Asn364, His367, Ser375, and Gln376 amino acid residues, which might explain the stronger binding of **1b** than kojic acid to hTYR. The docking score of **1b** was − 7.0 kcal/mol (Fig. 6b). On the other hand, compound **1f** showed a binding pattern similar to that with mTYR. No metal interaction with zinc ions was observed, and only one hydrogen bond was observed between Asn364 and the 3-hydroxyl group on its phenyl ring. Interestingly, the DHIT moiety of **1f** interacted with a negatively charged amino acid (Asp199) as shown in 2D in Fig. 6a. The docking score of **1f** was − 3.9 kcal/mol. In summary, derivatives **1b** and **1f** were both found to bind directly with the mTYR and hTYR homology models, and docking simulations of both derivatives with the mTYR and the hTYR homology model were similar.

2.2.4. Cell study

Since **1b** and **1f** exhibited potent TYR inhibitory activity at the enzyme level, we investigated whether they also inhibited TYR at the cellular level using B16F10 murine melanoma cells.

2.2.4.1. Cell cytotoxicity study. Before examining inhibitory effects of compounds **1b** and **1f** on cellular tyrosinase activity, we examined their cytotoxic effects on B16F10 murine cells using the EZ-cytox assay (Daeil Lab Service, Seoul, Korea). After B16F10 cells had been cultured for 24 h, cells were treated with different concentrations (0, 1, 2, 5, 10 or 20 μM) of **1b** or **1f** for 48 h in a humidified atmosphere. Optical densities (ODs) were measured at 450 nm using a microplate reader.

Cytotoxicity results are shown in Fig. 7. Neither **1b** nor **1f** had a significant cytotoxic effect on B16F10 cells at concentrations up to 20 μM. Therefore, subsequent cell-based assays on TYR inhibition and intracellular melanogenesis were performed using **1b** and **1f** concentrations of ≤ 20 μM.

2.2.4.2. Cellular tyrosinase inhibition. B16F10 cells co-stimulated with α -melanocyte-stimulating hormone (α -MSH) and 3-isobutyl-1-methylxanthine (IBMX) were used to investigate the inhibitory effects of compounds **1b** and **1f** on mammal cellular tyrosinase. Kojic acid was used as the positive control. After incubation for 24 h, B16F10 melanoma cells were pretreated with 20 μM of kojic acid or derivatives **1b** or **1f** at concentrations of 0, 5, 10, or 20 μM for 1 h and then co-treated with 1 μM of α -MSH and 200 μM of IBMX for 48 h to enhance tyrosinase activity. Cellular tyrosinase activities were determined by measuring optical densities at 492 nm.

Cellular tyrosinase activity results for derivatives **1b** and **1f** are shown in Fig. 8. Exposure of B16F10 cells to α -MSH and IBMX significantly increased tyrosinase activity to 245% versus non-treated controls and pretreatment with **1b** or **1f** significantly and concentration-dependently reduced this increase in tyrosinase activity. Compound **1b** at 10 μM inhibited cellular TYR to the same extent as compound **1f** or kojic acid at 20 μM.

2.2.4.3. Intracellular melanin inhibition. To determine whether the inhibitory effects of compounds **1b** and **1f** on cellular TYR influence melanogenesis, cellular melanin production was measured. As was performed in TYR inhibition experiments, B16F10 cells co-stimulated with α -MSH and IBMX were used to compare the inhibitory effects of **1b** and **1f** on melanogenesis. Kojic acid was used as the positive control. After incubation for 24 h, B16F10 melanoma cells were pretreated with kojic acid at 20 μM or compounds **1b** or **1f** at 0, 5, 10, or 20 μM for 1 h, and then co-treated with 1 μM of α -MSH and 200 μM of IBMX for 48 h to increase melanin production. Intracellular melanin contents were determined by measuring optical densities at 405 nm.

Intracellular melanin content results are provided in Fig. 9. Co-treatment with α -MSH and IBMX increased melanin production to 285% *vs.* non-treated controls but pretreatment with **1b** or **1f** significantly and concentration-dependently suppressed this increase. Compound **1b** at 5 μM suppressed intracellular melanin production by the same extent as kojic acid at 20 μM, and at 20 μM, compound **1f** had a stronger inhibitory effect on melanogenesis than kojic acid.

Furthermore, these inhibitory effects on intracellular melanin contents were similar to those observed on intracellular tyrosinase
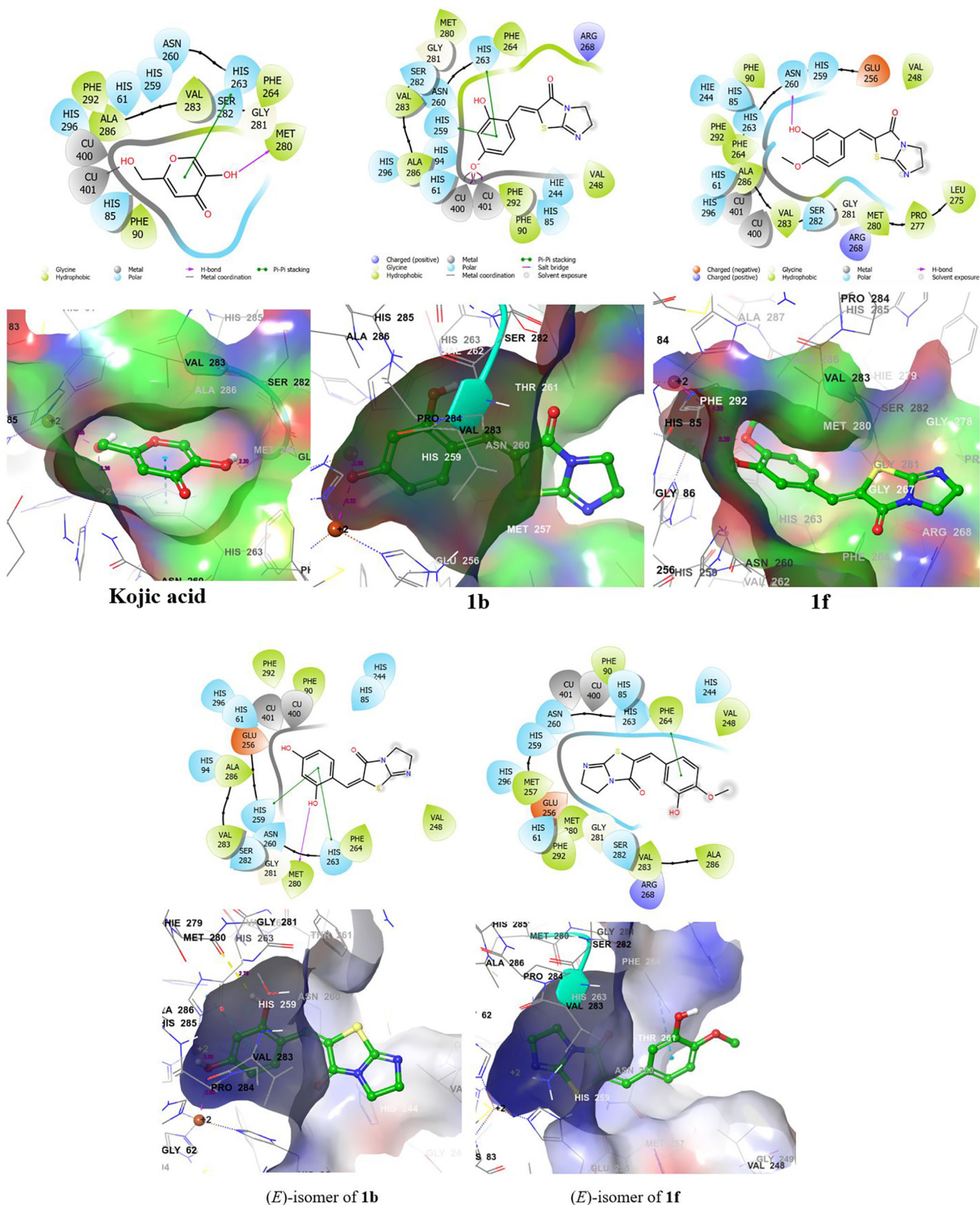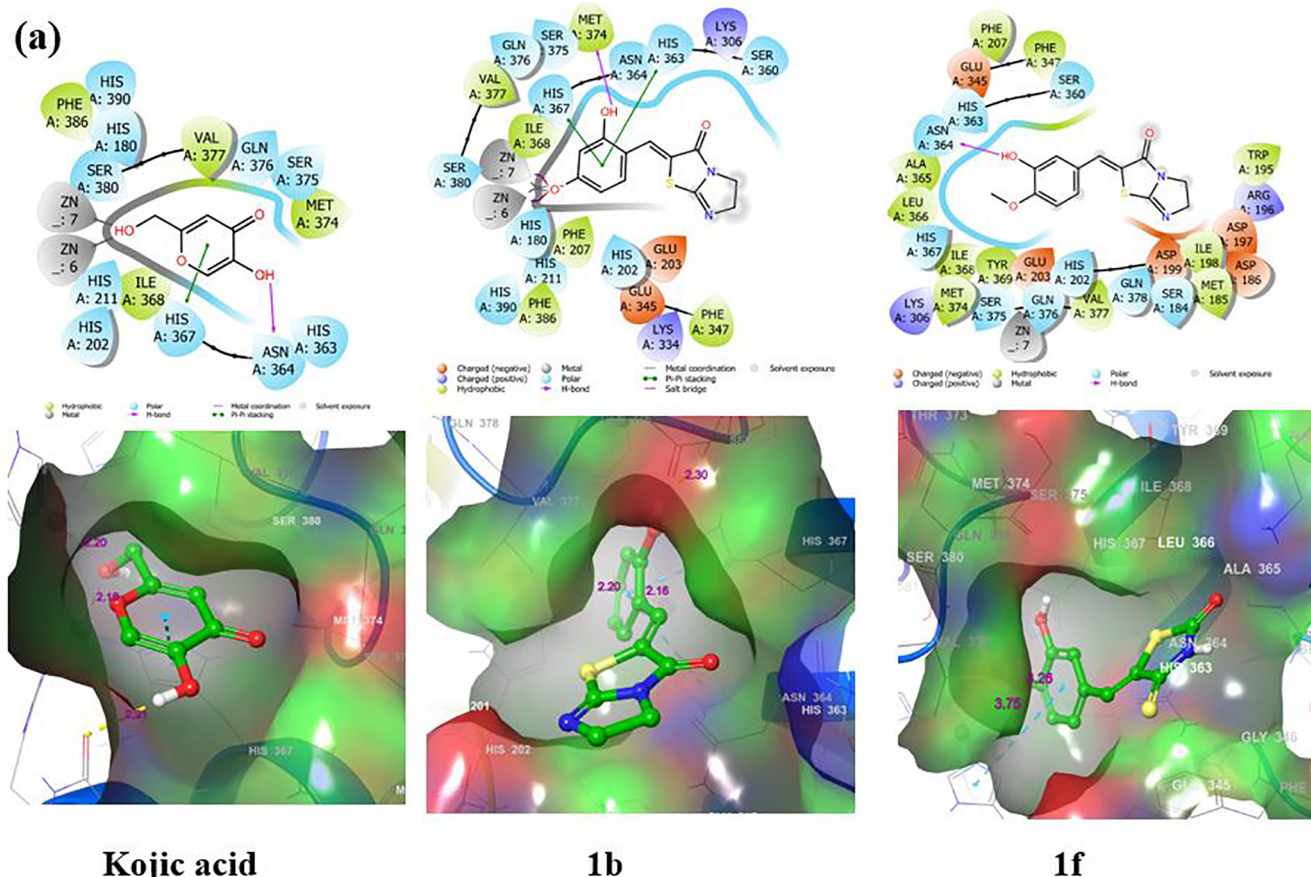
Fig. 5a. Docking studies on derivatives **1b** or **1f** or kojic acid using Schrödinger suite. *m*TYR (*Agaricus bisporus* tyrosinase, PDB ID = 2Y9X) was used as the tyrosinase for docking simulations. Pharmacophore results for **1b**, **1f**, and kojic acid are represented in 2D and 3D.

Fig. 5b. Docking studies on the (*E*)-isomers of **1b** and **1f** using Schrödinger suite. *m*TYR (*Agaricus bisporus* tyrosinase, PDB ID = 2Y9X) was used as the tyrosinase for docking simulations. Pharmacophore results for **1b** and **1f** are represented in 2D and 3D.

activity, which indicated the anti-melanogenesis effects of **1b** and **1f** were caused by their TYR inhibitory effects.

2.2.4.4. Inhibition of extracellular melanin levels. To determine whether melanin levels in cell culture media were influenced by compounds **1b** or **1f**, melanin contents in B16F10 cell culture media after treatments with derivatives at different concentrations in the presence of α -MSH and IBMX for 48 h were analyzed by measuring optical densities at 405 nm using a microplate reader.

Melanin levels in media are shown in Fig. 10. These levels were increased by co-treatment with α -MSH and IBMX to 178% *vs.* non-treated controls. However, pretreatment with **1b** or **1f** significantly and concentration-dependently suppressed these increases. Compound **1b** at 5 μM and compound **1f** at 20 μM suppressed these increases more than kojic acid at 20 μM. These results were similar

to those obtained for intracellular melanin contents and indicate that **1b** and **1f** both reduced intracellular melanin contents and melanin release to the extracellular compartment.

3. Conclusions

Eleven 5,6-dihydroimindazo[2,1-*b*]thiazol-3(2*H*)-one (DHIT) derivatives bearing various benzylidene groups were designed and synthesized as potential tyrosinase inhibitors. Three derivatives (compounds **1a**, **1b**, and **1f**) were found to inhibit mushroom tyrosinase more than kojic acid, and compound **1b** with a 2,4-dihydroxyphenyl ring had an IC_{50} value $\sim$ 100-fold lower than kojic acid. Kinetic studies demonstrated that compounds **1b** and **1f**, which both inhibited mushroom tyrosinase activity more than kojic acid, were competitive inhibitors. In silico docking simulation
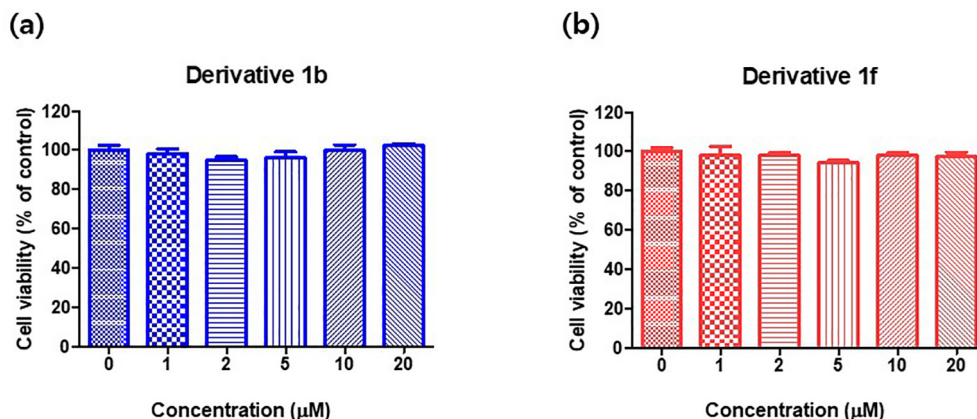
Fig. 6. Expected binding modes and docking scores of the DHIT derivatives **1b** or **1f** or kojic acid as determined using the *h*TYR homology model and Schrödinger suite. (a) 2D and 3D representations of **1b**, **1f**, and kojic acid, and (b) the binding affinities of **1b**, **1f**, and kojic acid for mushroom tyrosinase (PDB: 2Y9X) and the human tyrosinase homology model.
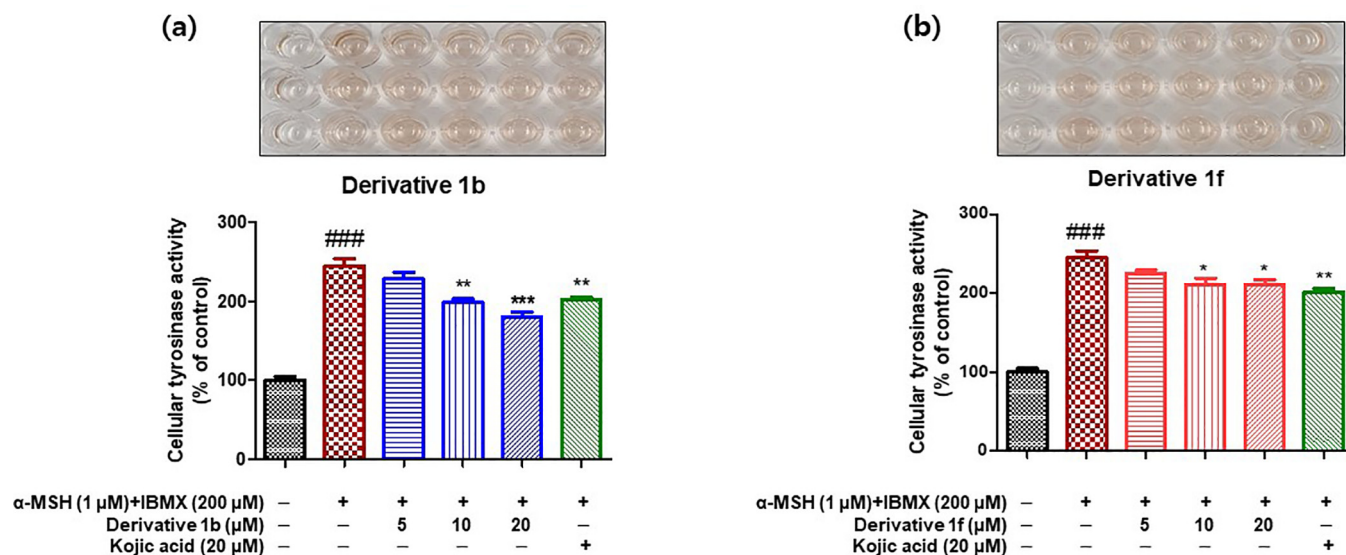

Fig. 7. Viabilities of B16F10 cells treated with compounds **1b** (a) or **1f** (b). Cell viability experiments were performed at concentrations of 0, 1, 2, 5, 10, or 20 μM of **1b** or **1f** using an EZ-cytox assay method. Cells were treated with **1b** and **1f** for 48 h and optical densities were measured after treatment with EZ-cytox solution for 1 h. Results are presented as the means ± standard errors of five independent experiments.

results supported that **1b** and **1f** compete with L-tyrosine (a tyrosinase substrate) for the active site of tyrosinase. Cell-based experiments performed on B16F10 melanoma cells demonstrated that compounds **1b** and **1f** suppressed melanogenesis more than kojic acid due to their greater inhibitory effects on cellular tyrosinase. Our *in silico* study conducted using a human tyrosinase homology model supported the notion that **1b** and **1f** are strong candidate anti-melanogenesis agents for the treatment of diseases associated with hyperpigmentation. Furthermore, these results suggest that DHIT might be a useful template for the development of novel and potent tyrosinase inhibitors.

4. Materials and methods

4.1. Chemistry

4.1.1. General methods

Reagents and chemicals were obtained commercially and used without further purification. All reactions were monitored by thin layer chromatography (TLC) using Merck precoated 60F$_{245}$ plates, and reaction mixtures were purified by column chromatography using MP Silica 40–63 (60 Å). Mass spectroscopy was performed in electrospray ionization (ESI) positive mode using an Expression CMA spectrometer (Advion Ithaca, NY, USA). ^{1}H NMR (400 and 500 MHz) and ^{13}C NMR (100 and 125 MHz) data were obtained using a Varian Unity INOVA 400 spectrometer or a Varian Unity AS500 spectrometer (Agilent Technologies, Santa Clara, CA, USA). DMSO d_6 and CDCl$_3$ were used as NMR solvents. Chemical shift values were recorded in parts per million (ppm) and coupling constants (*J*) were recorded in hertz (Hz). The following abbreviations are used: s (singlet), d (doublet), t (triplet), q (quartet), m (multiplet), and brs (broad singlet).

4.1.2. Synthesis of 5,6-dihydroimidazo[2,1-b]thiazol-3(2H)-one (**2**).

To a stirred solution of 2-thioimidazolidine (5.00 g, 48.94 mmol) and sodium acetate (20.07 g, 244.67 mmol) in EtOH (150 mL) was added ethyl chloroacetate (10.47 mL, 97.82 mmol) at 0 °C. The reaction mixture was refluxed for 21 h and cooled, and the precipitate obtained was removed by filtration, washed with EtOH, and the filtrate was partitioned between dichloromethane and water. The organic layer was concentrated *in vacuo* and the resultant residue was purified by silica gel column chromatography using
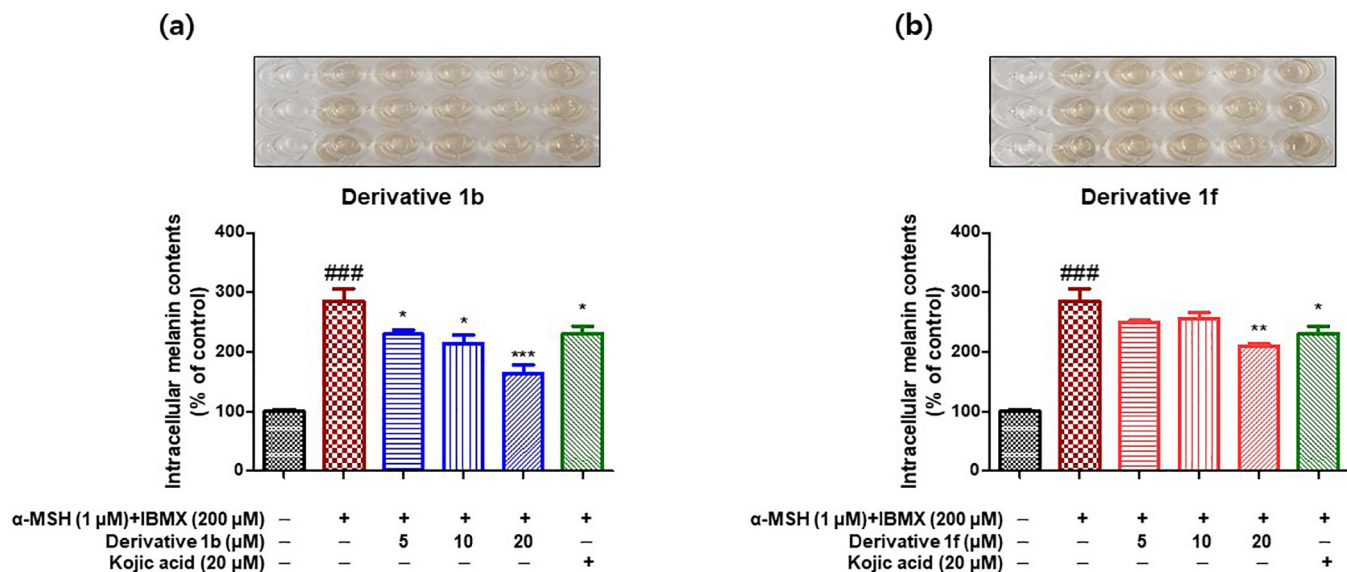
(a)

(b)

Fig. 8. Inhibitory effects of compounds **1b** (a) and **1f** (b) on tyrosinase in B16F10 cells. Cells were stimulated by co-treating them with α -MSH (1 μM) and IBMX (200 μM) and then treated with compounds **1b** or **1f** at 0, 5, 10, or 20 μM, or kojic acid at 20 μM for 48 h. Cellular tyrosinase activities were determined by measuring optical densities at 492 nm. Results are presented as the means ± standard errors of experiments conducted in triplicate. [###]$P < 0.001$ *vs.* non-treated controls; [*]$P < 0.05$, [**]$P < 0.01$, [***]$P < 0.001$ *vs.* α -MSH and IBMX-treated cells.
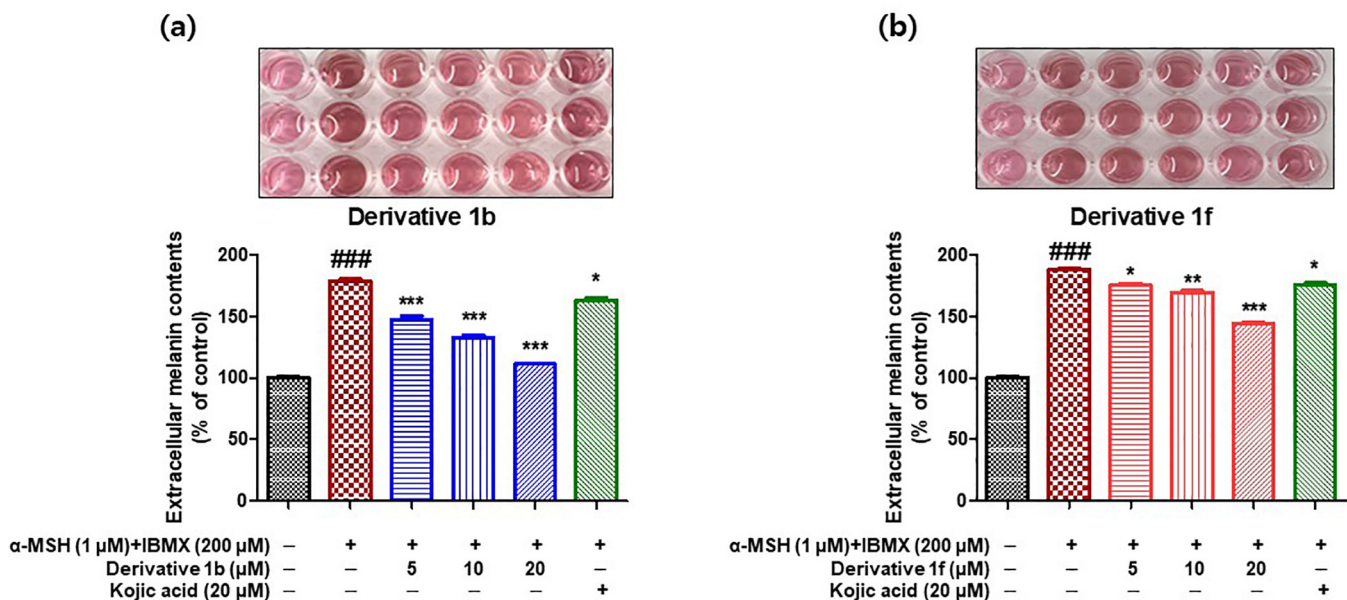
(a)

(b)

Fig. 9. Inhibitory effects of compounds **1b** (a) and **1f** (b) on the melanin contents of B16F10 cells. Cells were stimulated by co-treating them with α -MSH (1 μM) and IBMX (200 μM) and then treated with 0, 5, 10, or 20 μM of **1b** or **1f**, or 20 μM of kojic acid for 48 h. Intracellular melanin contents were determined by measuring optical densities at 405 nm. Results are presented as the means ± standard errors of experiments performed in triplicate. [###]$P < 0.001$ *vs.* non-treated controls; [*]$P < 0.05$, [**]$P < 0.01$, [***]$P < 0.001$, *vs.* α -MSH and IBMX-treated cells.

dichloromethane and methanol (20:1) as eluent to give 5,6-dihydroimidazo[2,1-*b*]thiazol-3(2*H*)-one (**2**, 5.00 g) as a white solid (yield 71.9%).

^{1}H NMR (400 MHz, CDCl$_3$) δ 4.33 (t, 2H, J = 8.8 Hz, 5-H$_2$), 4.12 (s, 2H, 2-H$_2$), 3.69 (t, 2H, J = 8.8 Hz, 6-H$_2$); ^{13}C NMR (125 MHz, CDCl$_3$) δ 164.7, 161.8, 61.8, 41.6, 39.7.

4.1.3. General synthetic procedure for (Z)-2-(substituted benzylidene)-5,6-dihydroimidazo[2,1-b]thiazol-3(2H)-one derivatives (1a – 1 k).

A solution of **2** (100 mg, 0.70 mmol), benzaldehyde (1 equiv.), and NaOAc (173 mg, 2.11 mmol) in acetic acid (1.0 mL) was heated

at 80 °C for 2 – 12 h, cooled, and water (5 mL) was added. The precipitates formed were filtered, and washed with water to give **1a** – **1 k** as a solid in yields of 36.9 – 87.5%.

4.1.3.1. (Z)-2-(4-Hydroxybenzylidene)-5,6-dihydroimidazo[2,1-b]thi-azol-3(2H)-one (1a). 67.9%; ^{1}H NMR (500 MHz, DMSO d_6) δ 10.18 (brs, 1H, OH), 7.55 (s, 1H, vinylic H), 7.43 (d, 2H, J = 8.5 Hz, 2′-H, 6′-H), 6.90 (d, 2H, J = 8.5 Hz, 3′-H, 5′-H), 4.28 (t, 2H, J = 8.5 Hz, 5-H$_2$), 3.78 (t, 2H, J = 8.5 Hz, 6-H$_2$); ^{13}C NMR (125 MHz, DMSO d_6) δ 160.4, 159.7, 157.3, 132.1, 130.4, 124.5, 123.5, 116.7, 61.2, 42.0; LRMS (ESI +) m/z 247 (M + H)$^+$.
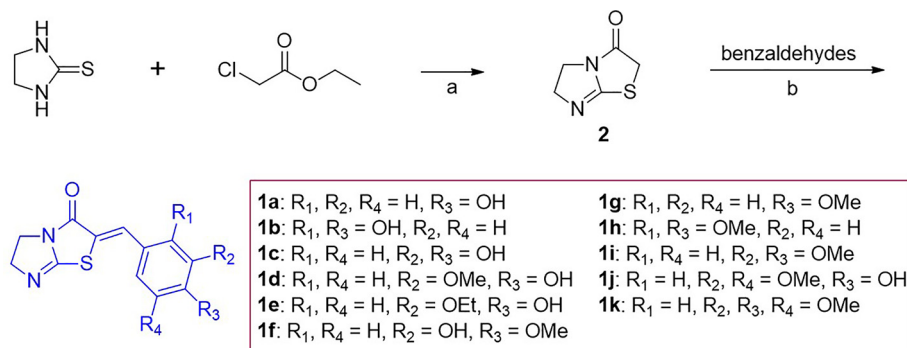
Fig. 10. The inhibitory effects of compounds **1b** (a) and **1f** (b) on the release of melanin to medium by B16F10 cells. Cells were stimulated by co-treating them with α -MSH (1 μM) and IBMX (200 μM), and then incubated with compounds **1b** or **1f** at 0, 5, 10, or 20 μM or kojic acid at 20 μM for 48 h. Melanin levels in media were determined by measuring optical densities at 405 nm. Results are presented as the means ± standard errors of experiments performed in triplicate. ###P < 0.001 *vs.* non-treated controls; *P < 0.05, **P < 0.01, ***P < 0.001 *vs.* α -MSH and IBMX-treated cells.

4.1.4. 2. (Z)-2-(2,4-Dihydroxybenzylidene)-5,6-dihydroimidazo[2,1-b] thiazol-3(2H)-one (1b)

59.4%; ^{1}H NMR (500 MHz, DMSO d_6) δ 10.30 (s, 1H, OH), 10.01 (s, 1H, OH), 7.79 (s, 1H, vinylic H), 7.16 (d, 1H, J = 9.0 Hz, 6'-H), 6.39 (s, 1H, 3'-H), 6.37 (d, 1H, J = 9.0 Hz, 5'-H), 4.24 (t, 2H, J = 8.0 Hz, 5-H$_2$), 3.75 (t, 2H, J = 8.0 Hz, 6-H$_2$); ^{13}C NMR (100 MHz, DMSO d_6) δ 161.6, 161.0, 159.3, 157.8, 129.9, 125.9, 121.8, 112.3, 108.6, 103.2, 61.3, 42.2; LRMS (ESI +) m/z 263 (M + H)$^+$.

4.1.4.1. (Z)-2-(3,4-Dihydroxybenzylidene)-5,6-dihydroimidazo[2,1-b] thiazol-3(2H)-one (1c). 74.2%; ^{1}H NMR (400 MHz, DMSO d_6) δ 9.52 (brs, 2H, 2 × OH), 7.41 (s, 1H, vinylic H), 6.94 (s, 1H, 2'-H), 6.88 (d, 1H, J = 8.0 Hz, 6'-H), 6.82 (d, 1H, J = 8.0 Hz, 5'-H), 4.22 (t, 2H, J = 8.0 Hz, 5-H$_2$), 3.73 (t, 2H, J = 8.0 Hz, 6-H$_2$); ^{13}C NMR (100 MHz, DMSO d_6) δ 160.6, 157.6, 148.6, 146.4, 131.0, 125.1, 123.6, 123.5, 116.9, 116.6, 61.4, 42.2; LRMS (ESI +) m/z 263 (M + H)$^+$.

4.1.4.2. (Z)-2-(4-Hydroxy-3-methoxybenzylidene)-5,6-dihydroimi-dazo[2,1-b]thiazol-3(2H)-one (1d). 36.9%; ^{1}H NMR (400 MHz, DMSO d_6) δ 9.78 (s, 1H, OH), 7.52 (s, 1H, vinylic H), 7.11 (s, 1H, 2'-H), 7.00 (d, 1H, J = 8.0 Hz, 6'-H), 6.88 (d, 1H, J = 8.0 Hz, 5'-H), 4.24 (t, 2H, J = 8.0 Hz, 5-H$_2$), 3.78 (s, 3H, OCH$_3$), 3.72 (t, 2H, J = 8.0 Hz, 6-H$_2$); ^{13}C NMR (100 MHz, DMSO d_6) δ 160.5, 157.5, 149.4, 148.6, 131.0, 125.1, 124.0, 123.7, 116.8, 114.4, 61.5, 56.3, 42.2; LRMS (ESI +) m/z 277 (M + H)$^+$.

4.1.4.3. (Z)-2-(3-Ethoxy-4-hydroxybenzylidene)-5,6-dihydroimidazo [2,1-b]thiazol-3(2H)-one (1e). 71.8%; ^{1}H NMR (500 MHz, DMSO d_6) δ 7.53 (s, 1H, vinylic H), 7.11 (d, 1H, J = 1.5 Hz, 2'-H), 7.01 (dd, 1H, J = 8.5, 1.5 Hz, 6'-H), 6.91 (d, 1H, J = 8.5 Hz, 5'-H), 4.26 (t, 2H, J = 8.5 Hz, 5-H$_2$), 4.06 (q, 2H, J = 7.0 Hz, CH$_2$CH$_3$), 3.77 (t, 2H, J = 8.5 Hz, 6-H$_2$), 1.34 (t, 3H, J = 7.0 Hz, CH$_2$CH$_3$); ^{13}C NMR (100 MHz, DMSO d_6) δ 160.5, 157.5, 149.7, 147.7, 131.0, 125.1, 123.9, 123.8, 116.8, 115.4, 64.5, 61.5, 42.2, 15.3; LRMS (ESI +) m/z 291 (M + H)$^+$.

4.1.4.4. (Z)-2-(3-Hydroxy-4-methoxybenzylidene)-5,6-dihydroimi-dazo[2,1-b]thiazol-3(2H)-one (1f). 62.9%; ^{1}H NMR (500 MHz, DMSO d_6) δ 9.45 (s, 1H, OH), 7.49 (s, 1H, vinylic H), 7.06 (d, 1H, J = 9.0 Hz, 6'-H), 7.04 (d, 1H, J = 9.0 Hz, 5'-H), 7.01 (s, 1H, 2'-H), 4.27 (t, 2H, J = 8.0 Hz, 5-H$_2$), 3.82 (s, 3H, OCH$_3$), 3.78 (t, 2H, J = 8.0 Hz, 6-H$_2$); ^{13}C NMR (125 MHz, DMSO d_6) δ 160.2, 157.2, 149.9, 147.3, 130.4, 126.2, 124.6, 122.9, 116.0, 112.9, 61.2, 56.1, 42.0; LRMS (ESI +) m/z 277 (M + H)$^+$.

4.1.4.5. (Z)-2-(4-Methoxybenzylidene)-5,6-dihydroimidazo[2,1-b]thi-azol-3(2H)-one (1 g). 65.2%; ^{1}H NMR (500 MHz, CDCl$_3$) δ 7.64 (s, 1H, vinylic H), 7.44 (d, 2H, J = 8.0 Hz, 2'-H, 6'-H), 6.98 (d, 2H, J = 8.0 Hz, 3'-H, 5'-H), 4.42 (t, 2H, J = 8.0 Hz, 5-H$_2$), 3.87 (t, 2H, J = 8.0 Hz, 6-H$_2$), 3.85 (s, 3H, OCH$_3$); ^{13}C NMR (125 MHz, CDCl$_3$) δ 160.9, 160.9, 159.0, 131.5, 131.2, 126.0, 124.3, 114.6, 60.9, 55.4, 41.8; LRMS (ESI +) m/z 261 (M + H)$^+$.

4.1.4.6. (Z)-2-(2,4-Dimethoxybenzylidene)-5,6-dihydroimidazo[2,1-b] thiazol-3(2H)-one (1 h). 72.7%; ^{1}H NMR (500 MHz, CDCl$_3$) δ 7.97 (s, 1H, vinylic H), 7.37 (d, 1H, J = 9.0 Hz, 6'-H), 6.56 (dd, 1H, J = 9.0, 2.5 Hz, 5'-H), 6.46 (d, 1H, J = 2.0 Hz, 3'-H), 4.39 (t, 2H, J = 8.5 Hz, 5-H$_2$), 3.86 (s, 3H, OCH$_3$), 3.85 (t, 2H, J = 8.5 Hz, 6-H$_2$), 3.84 (s, 3H, OCH$_3$); ^{13}C NMR (100 MHz, CDCl$_3$) δ 162.9, 161.4, 159.9, 159.7, 130.3, 127.0, 124.5, 115.8, 105.3, 98.8, 61.0, 55.7, 55.7, 42.1; LRMS (ESI +) m/z 291 (M + H)$^+$.

4.1.4.7. (Z)-2-(3,4-Dimethoxybenzylidene)-5,6-dihydroimidazo[2,1-b] thiazol-3(2H)-one (1i). 87.5%; ^{1}H NMR (500 MHz, CDCl$_3$) δ 7.60 (s, 1H, vinylic H), 7.08 (dd, 1H, J = 8.0, 2.0 Hz, 6'-H), 6.97 (d, 1H, J = 2.0 Hz, 2'-H), 6.93 (d, 1H, J = 8.0 Hz, 5'-H), 4.40 (t, 2H, J = 8.5 Hz, 5-H$_2$), 3.91 (s, 6H, 2 × OCH$_3$), 3.85 (t, 2H, J = 8.5 Hz, 6-H$_2$); ^{13}C NMR (100 MHz, CDCl$_3$) δ 161.0, 158.8, 150.7, 149.4, 131.4, 126.5, 124.9, 123.7, 112.3, 111.5, 61.3, 56.2, 56.1, 42.0; LRMS (ESI +) m/z 291 (M + H)$^+$.

4.1.4.8. (Z)-2-(4-Hydroxy-3,5-dimethoxybenzylidene)-5,6-dihydroim-idazo[2,1-b]thiazol-3(2H)-one (1j). 54.5%; ^{1}H NMR (500 MHz, DMSO d_6) δ 9.20 (brs, 1H, OH), 7.56 (s, 1H, vinylic H), 6.86 (s, 2H, 2'-H, 6'-H), 4.28 (t, 2H, J = 8.5 Hz, 5-H$_2$), 3.82 (s, 6H, 2 × OCH$_3$), 3.79 (t, 2H, J = 8.5 Hz, 6-H$_2$); ^{13}C NMR (100 MHz, DMSO d_6) δ 160.5, 157.4, 148.9, 138.6, 131.2, 124.4, 124.0, 108.0, 61.5, 56.7, 42.3; LRMS (ESI +) m/z 307 (M + H)$^+$.

4.1.4.9. (Z)-2-(3,4,5-Trimethoxybenzylidene)-5,6-dihydroimidazo[2,1-b]thiazol-3(2H)-one (1 k). 78.2%; ^{1}H NMR (400 MHz, CDCl$_3$) δ 7.58 (s, 1H, vinylic H), 6.69 (s, 2H, 2'-H, 6'-H), 4.41 (t, 2H, J = 8.4 Hz, 5-H$_2$), 3.88 (s, 6H, 2 × OCH$_3$), 3.87 (s, 3H, 4'–OCH$_3$), 3.87 (t, 2H, J = 8.4 Hz, 6-H$_2$); ^{13}C NMR (100 MHz, CDCl$_3$) δ 160.7, 159.0, 153.8, 139.9, 131.8, 129.0, 126.4, 107.1, 61.2, 61.1, 56.4, 42.1; LRMS (ESI +) m/z 321 (M + H)$^+$.

4.2. Tyrosinase inhibition - Kinetics, mechanism, and in silico and in vitro studies

4.2.1. Mushroom tyrosinase inhibition assay

The tyrosinase inhibitory activity assays on the synthesized DHIT derivatives **1a** – **1 k** was performed using mushroom tyrosinase (*m*TYR), as previously described [72] with minor modification. Briefly, a 200 μL mixture containing tyrosinase solution (20 μL, 200 units), a DHIT derivative (10 μL, final concentration 25 μM), and

substrate solution (170 μL, comprising 14.7 mM potassium phosphate buffer and 293 μM L-tyrosine solution (1:1, v/v)) was added to a 96-well microplate and incubated for 30 min at 37 °C. The optical densities of dopachrome produced during incubation were measured using a microplate reader (VersaMax™, Molecular Devices, Sunnyvale, CA, USA) at 492 nm. Kojic acid (25 μM) was used as the positive control. All experiments were conducted in triplicate. To calculate the tyrosinase inhibitory activities, the following formula was used: % inhibition = $[(1 - (A/B)) \times 100]$, where A is test sample optical density and B is the optical density of the non-treated control.

To calculate the concentration required to inhibit enzyme activity by 50% (IC_{50}), tyrosinase inhibition percentages of each DHIT derivative were obtained at 5 or more different concentrations. IC_{50} values were calculated by plotting linear regression curves of percentage inhibitions versus derivative concentrations. The negative control was obtained by adding dimethyl sulfoxide (DMSO) instead of a DHIT derivative. Kojic acid was used as the positive control.

4.2.2. Kinetics of mTYR inhibitions by 1b and 1f

Lineweaver-Burk plots were used to determine modes of *m*TYR inhibition. Compounds **1b** or **1f** (10 μL, final concentrations: 0, 0.0625, 0.125, or 0.25 μM for **1b** and 0, 1, 2 or 4 μM for **1f**) and *m*TYR solution (20 μL, 150 units) were added to a 96-well plate containing 170 μL of a mixture containing aqueous L-tyrosine solution at final concentrations of 0.5, 1.0, 2.0, 4.0, 8.0, or 16 mM for **1b** or 1.0, 2.0, 4.0, or 8.0 mM for **1f**; aqueous L-tyrosine solution, distilled water, and 50 mM potassium phosphate buffer (pH 6.5) in the ratio 10:9:10. Initial rates of dopachrome formations in reaction mixtures were calculated by measuring increases in optical density at 492 nm (ΔOD_{492}/min) using a microplate reader (VersaMax™, Molecular Devices, Sunnyvale, CA, USA). Maximum velocities of tyrosinase-L-tyrosine reactions were determined using Lineweaver-Burk plots (inverse of reaction velocity (1/V) versus the inverse of L-tyrosine concentration (1/[S])) obtained using 4 – 5 different concentrations of L-tyrosine. Modes of tyrosinase inhibition were determined using convergence points of plots.

4.2.3. In silico study on interactions between tyrosinase and compounds 1b or 1f or kojic acid

4.2.3.1. In silico studies of interactions between mushroom tyrosinase and DHIT derivatives 1b and 1f.

Docking studies on compounds **1b** and **1f** and kojic acid were performed using Schrodinger suite (2021–1) as previously described protocols [73] with slight modification. The crystal structure of *m*TYR (PDB ID 2Y9X) was imported from the Protein Data Bank (PDB) using Maestro 12.4 Protein Preparation Wizard and prepared in protein preparation wizard by removing unwanted protein chains. To further refine the structure, hydrogen atoms were added, water molecules > 3 Å from the ligand were removed, and the structure was minimized. In minimized protein structures, glide grid and active sites were determined using the tyrosinase binding site obtained from the PDB and the literature [74-76]. The structures of **1b**, **1f**, and kojic acid were then imported into the entry list of Maestro in CDXML format. Prior to ligand docking, the structures of **1b**, **1f**, and kojic acid were developed using LigPrep. Compounds were then docked to the glide grid using Glide from the Maestro task list [77]. Binding affinities and ligand–protein interactions were obtained using the glide extra precision (XP) method [78].

4.2.3.2. In silico studies of interactions between the hTYR homology model and 1b, 1f, and kojic acid.

For *in silico* studies on DHIT derivates **1b** and **1f** an *h*TYR homology model was created using the Swiss model Online Server and Schrodinger Suite (2020–2). The *h*TYR (P14679) protein sequence was imported from the UniProt database and a homology model was developed on the Swiss model online server using the human TRP1 (PDB: 5M8Q) template. The model was further processed using Schrödinger suite and verified using Schrodinger Prime (a homology modeling tool in Schrödinger suite). Compounds **1b** and **1f** and kojic acid were docked to a processed human homology model using a protocol similar to that mentioned for *m*TYR docking.

4.2.4. Cell culture

B16F10 murine melanoma cells were acquired from the American Type Culture Collection (ATCC, Manassas, VA, USA) and cultured in Dulbecco's modified Eagle's medium (DMEM), supplemented with 10% fetal bovine serum (FBS) and 1% penicillin–streptomycin in a humidified 5% CO_2 atmosphere at 37 °C. These cells were used for cell viability, melanin content, and cellular tyrosinase activity assays in 96- or 6-well culture plates.

4.2.5. Cell viability analysis

Cell viability assays were performed at 37 °C as previously described [79] with minor modification using the EZ-cytox assay. In brief, B16F10 melanoma cells were seeded in 96-well plates at a density of 1×10^4 cells/well and incubated in a humidified 5% CO_2 atmosphere for 24 h at 37 °C. Cells were then treated with compounds **1b** or **1f** at 0, 1, 2, 5, 10, or 20 μM/well for 48 h. EZ-cytox solution (10 μL) (Daeil Lab Service, Seoul, Korea) was then added to each well and incubated for 1 h at 37 °C. Cell viabilities were assessed by measuring absorbances at 450 nm using a microplate reader (VersaMax™, Molecular Devices, Sunnyvale, CA, USA). All experiments were independently conducted three times.

4.2.6. Cellular tyrosinase inhibition assays of compounds 1b and 1f in B16F10 cells

Cellular tyrosinase inhibition assays were conducted as previously described [80] with minor modification. B16F10 cells were seeded at a density of 1×10^5 cells/well in 6-well plates and incubated in a humidified 5% CO_2 atmosphere for 24 h at 37 °C. Cultured B16F10 cells were then treated with **1b**, **1f**, or kojic acid dissolved in DMSO at final concentrations of 0, 5, 10, or 20 μM for **1b** and **1f** or 20 μM for kojic acid for 1 h. α-MSH (final concentration: 1 μM) and IBMX (final concentration: 200 μM) were then added, and cells were incubated in a humidified 5% CO_2 atmosphere for 48 h at 37 °C. Cells were then washed twice with PBS, lysed by adding 45 mM of phosphate buffer (100 μL) containing 1% Triton X-100 (5 μL) and 1% PMSF (5 μL, phenylmethylsulfonyl fluoride) and frozen at −80 °C for 1 h. Lysates were clarified by centrifugation at 12,000 rpm for 30 min at 4 °C. Cell lysate supernatants (80 μL/well) in a 96-well plate were then mixed with 20 μL of L-DOPA (2 mg/mL in distilled water) and incubated for 30 min at 37 °C. Absorbances of reaction mixtures at 492 nm were recorded using a microplate reader (VersaMax™, Molecular Devices, Sunnyvale, CA, USA). Kojic acid was used as the positive control. Protein concentrations were determined using Bicinchoninic Acid (BCA) protein assay reagent using Bovine Serum Albumin (BSA) as the standard (Thermo Scientific, Rockford, IL, USA). All experiments were independently conducted three times.

4.2.7. Determinations of intra- and extracellular melanin contents in B16F10 melanoma cells

The inhibitory effects of compounds **1b** and **1f** on intracellular melanin contents were investigated as previously described [81]. B16F10 cells were seeded at a density of 1×10^5 cells/well in 6-well plates and incubated in a humidified 5% CO_2 atmosphere for 24 h at 37 °C. DHIT derivatives were dissolved in DMSO, and cultured cells were pretreated with compound **1b** or **1f** at 0, 5, 10, or 20 μM, or kojic acid at 20 μM for 1 h, 1 μM of α-MSH and 200 μM of IBMX were then added, and cells were incubated in a

humidified 5% CO_2 atmosphere for 48 h at 37 °C. For extracellular melanin contents, the optical density of the cell culture media was directly measured at 405 nm. On the other hand, for intracellular melanin contents, the following procedure was performed. Briefly, after washing twice with PBS, adherent cells were detached by incubation in Trypsin/EDTA for 1 min. Pellets were dissolved in 100 μL of 1 N NaOH and then incubated for 1 h at 60 °C to dissolve the melanin. Intracellular melanin was quantified by measuring optical densities at 405 nm using a microplate reader (VersaMax^{TM}, Molecular Devices, Sunnyvale, CA, USA). Results were normalized versus cell pellet total protein using BCA protein assay reagent using BSA as the standard (Thermo Scientific, Rockford, IL, USA). The intracellular melanin contents were calculated using the following equation: $(\Delta OD_{sample}/\Delta OD_{control}) \times 100\%$; where ΔOD_{sample} = the optical density of the test compound, and $\Delta OD_{control}$ = the optical density of control. Experiments were performed in triplicate.

4.2.8. Statistical analysis

Statistical analysis was carried out using GraphPad Prism (La Jolla, CA, USA) and results are presented as means ± standard errors of means (SEMs). One-way analysis of variance (ANOVA) followed by the Bonferroni post hoc test was used to determine the significances of intergroup differences. Statistical significance was accepted for P values < 0.05.

Declaration of Competing Interest

The authors declare that they have no known competing financial interests or personal relationships that could have appeared to influence the work reported in this paper.

Acknowledgment

Appendix A. Supplementary data

Supplementary data to this article can be found online at https://doi.org/10.1016/j.csbj.2022.02.007.

References

[1] Olivares C, Solano F. New insights into the active site structure and catalytic mechanism of tyrosinase and its related proteins. Pigment Cell Melanoma Res 2009;22(6):750–60.

[2] Fogal S, Carotti M, Giaretta L, Lanciai F, Nogara L, Bubacco L, et al. Human Tyrosinase Produced in Insect Cells: A Landmark for the Screening of New Drugs Addressing its Activity. Mol Biotechnol 2015;57(1):45–57.

[3] Ito S. A Chemist's View of Melanogenesis. Pigment Cell Res 2003;16(3):230–6.

[4] Maymone MBC, Neamah HH, Wirya SA, Patzelt NM, Secemsky EA, Zancanaro PQ, et al. The impact of skin hyperpigmentation and hyperchromia on quality of life: A cross-sectional study. J Am Acad Dermatol 2017;77(4):775–8.

[5] Roulier B, Pérès B, Haudecoeur R. Advances in the Design of Genuine Human Tyrosinase Inhibitors for Targeting Melanogenesis and Related Pigmentations. J Med Chem 2020;63(22):13428–43.

[6] Nazir Y, Rafique H, Kausar N, Abbas Q, Ashraf Z, Rachtanapun P, et al. Methoxy-Substituted Tyramine Derivatives Synthesis, Computational Studies and Tyrosinase Inhibitory Kinetics. Molecules 2021;26(9):2477. https://doi.org/10.3390/molecules26092477.

[7] Nazir Y, Saeed A, Rafiq M, Afzal S, Ali A, Latif M, et al. Hydroxyl substituted benzoic acid/cinnamic acid derivatives: Tyrosinase inhibitory kinetics, anti-melanogenic activity and molecular docking studies. Bioorg Med Chem Lett 2020;30(1):126722.

[8] Rafiq M, Nazir Y, Ashraf Z, Rafique H, Afzal S, Mumtaz A, et al. Synthesis, computational studies, tyrosinase inhibitory kinetics and antimelanogenic activity of hydroxy substituted 2-[(4-acetylphenyl)amino]-2-oxoethyl derivatives. J Enzyme Inhib Med Chem 2019;34(1):1562–72.

[9] Ashraf Z, Rafiq M, Nadeem H, Hassan M, Afzal S, Waseem M, et al. Carvacrol derivatives as mushroom tyrosinase inhibitors; synthesis, kinetics mechanism and molecular docking studies. PLoS One 2017;12(5):e0178069.

[10] Ashraf Z, Rafiq M, Seo S-Y, Kwon KS, Babar MM, Sadaf Zaidi N-u-S. Kinetic and in silico studies of novel hydroxy-based thymol analogues as inhibitors of mushroom tyrosinase. Eur J Med Chem 2015;98:203–11.

[11] Ashraf Z, Rafiq M, Seo S-Y, Babar MM, Zaidi N-u-SS. Synthesis, kinetic mechanism and docking studies of vanillin derivatives as inhibitors of mushroom tyrosinase. Bioorg Med Chem 2015;23(17):5870–80.

[12] Gonçalez ML, Corrêa MA, Chorilli M. Skin delivery of kojic acid-loaded nanotechnology-based drug delivery systems for the treatment of skin aging. Biomed Res Int 2013;2013:1–9.

[13] Kumar KS, Vani MG, Wang SY, Liao JW, Hsu LS, Yang HL, et al. In vitro and in vivo studies disclosed the depigmenting effects of gallic acid: A novel skin lightening agent for hyperpigmentary skin diseases. BioFactors 2013;39(3):259–70.

[14] Arndt KA, Fitzpatrick TB. Topical use of hydroquinone as a depigmenting agent. JAMA 1965;194(9):965–7.

[15] Fitzpatrick T, Arndt K, El Mofty A, Pathak M. Hydroquinone and psoralens in the therapy of hypermelanosis and vitiligo. Arch Dermatol 1966;93(5):589–600.

[16] Heilgemeir G, Balda B. Irreversible toxic depigmentation. Observations following use of hydroquinonemonobenzylether-containing skin bleaching preparations. MMW. Munchener medizinische Wochenschrift 1981;123(2):47.

[17] Kligman AM, Willis I. A new formula for depigmenting human skin. Arch Dermatol 1975;111(1):40–8.

[18] Breathnach AC, Nazzaro-Porro M, Passi S, Zina G. Azelaic acid therapy in disorders of pigmentation. Clin Dermatol 1989;7(2):106–19.

[19] Garcia-Lopez M. Double-blind comparison of azelaic acid and hydroquinone in the treatment of melasma. Acta Derm Venereol (Stockh) 1989;143:58–61.

[20] Khemis A, Kaiafa A, Queille-Roussel C, Duteil L, Ortonne J. Evaluation of efficacy and safety of rucinol serum in patients with melasma: a randomized controlled trial. Br J Dermatol 2007;156(5):997–1004.

[21] Köpke D, Mueller RH, Pyo SM. Phenylethyl resorcinol smartLipids for skin brightening–Increased loading & chemical stability. Eur J Pharm Sci 2019;137:104992.

[22] Mann T, Scherner C, Röhm K-H, Kolbe L. Structure-activity relationships of thiazolyl resorcinols, potent and selective inhibitors of human tyrosinase. Int J Mol Sci 2018;19(3):690.

[23] Kim Y-J, Uyama H. Tyrosinase inhibitors from natural and synthetic sources: structure, inhibition mechanism and perspective for the future. Cellular and Molecular Life Sciences CMLS 2005;62(15):1707–23.

[24] Chang T-S. An updated review of tyrosinase inhibitors. Int J Mol Sci 2009;10(6):2440–75.

[25] Cabanes J, Chazarra S, Garcia-carmona F. Kojic acid, a cosmetic skin whitening agent, is a slow-binding inhibitor of catecholase activity of tyrosinase. J Pharm Pharmacol 1994;46(12):982–5.

[26] Shin N-H, Ryu SY, Choi EJ, Kang S-H, Chang IL-M, Min KR, et al. Oxyresveratrol as the potent inhibitor on dopa oxidase activity of mushroom tyrosinase. Biochem Biophys Res Commun 1998;243(3):801–3.

[27] Khatib S, Nerya O, Musa R, Shmuel M, Tamir S, Vaya J. Chalcones as potent tyrosinase inhibitors: the importance of a 2, 4-substituted resorcinol moiety. Bioorg Med Chem 2005;13(2):433–41.

[28] Jung HJ, Lee MJ, Park YJ, Noh SG, Lee AK, Moon KM, et al. A novel synthetic compound,(Z)-5-(3-hydroxy-4-methoxybenzylidene)-2-iminothiazolidin-4-one (MHY773) inhibits mushroom tyrosinase. Biosci Biotechnol Biochem 2018;82(5):759–67.

[29] Kim SJ, Yang J, Lee S, Park C, Kang D, Akter J, et al. The tyrosinase inhibitory effects of isoxazolone derivatives with a (Z)-β-phenyl-α, β-unsaturated carbonyl scaffold. Bioorg Med Chem 2018;26(14):3882–9.

[30] S.J.K. Do Hyun Kim, S. Ullah, H.Y. Yun, P. Chun, H.R. Moon, Design, synthesis, and antimelanogenic effects of (2-substituted phenyl-1, 3-dithiolan-4-yl) methanol derivatives, Drug design, development and therapy 11 (2017) 827.

[31] H.Y. Yun, S.S. Do Hyun Kim, S. Ullah, S.J. Kim, Y.-J. Kim, J.-W. Yoo, Y. Jung, P. Chun, H.R. Moon, Design, synthesis, and anti-melanogenic effects of (E)-2-benzoyl-3-(substituted phenyl) acrylonitriles, Drug design, development and therapy 9 (2015) 4259.

[32] Pillaiyar T, Manickam M, Namasivayam V. Skin whitening agents: medicinal chemistry perspective of tyrosinase inhibitors. J Enzyme Inhib Med Chem 2017;32(1):403–25.

[33] Pillaiyar T, Manickam M, Jung S-H. Recent development of signaling pathways inhibitors of melanogenesis. Cell Signal 2017;40:99–115.

[34] Pillaiyar T, Namasivayam V, Manickam M, Jung SH. Inhibitors of Melanogenesis: An Updated Review. J Med Chem 2018;61(17):7395–418.

[35] Pillaiyar T, Manickam M, Jung SH. Downregulation of melanogenesis: drug discovery and therapeutic options. Drug Discov Today 2017;22(2):282–98.

[36] Halaouli S, Asther M, Sigoillot JC, Hamdi M, Lomascolo A. Fungal tyrosinases: new prospects in molecular characteristics, bioengineering and biotechnological applications. J Appl Microbiol 2006;100(2):219–32.

[37] M.K.A.H.T. Oba, Tyrosinase inhibitors, US201440112878A1, 2013.

[38] Boatman RJ, English JC, Perry LG, Bialecki VE. Differences in the nephrotoxicity of hydroquinone among Fischer 344 and Sprague-Dawley rats and B6C3F1 mice. J Toxicol Environ Health 1996;47(2):159–72.

[39] Afshin A, Forouzanfar MH, Reitsma MB, Sur P, Estep K, Lee A, et al. Health Effects of Overweight and Obesity in 195 Countries over 25 Years. The New England journal of medicine 2017;377(1):13–27.

[40] Barneda-Zahonero B, Parra M. Histone deacetylases and cancer. Mol Oncol 2012;6(6):579–89.

[41] Bang SH, Han SJ, Kim DH. Hydrolysis of arbutin to hydroquinone by human skin bacteria and its effect on antioxidant activity. Journal of cosmetic dermatology 2008;7(3):189–93.

[42] Coiffard C, Coiffard Lm, De Roeck-Holtzhauer Y. Degradation kinetics of arbutin in solution. Pharmazeutische Industrie 1999;61(6):574–6.

[43] Ha YM, Kim J-A, Park YJ, Park D, Kim JM, Chung KW, et al. Analogs of 5-(substituted benzylidene)hydantoin as inhibitors of tyrosinase and melanin formation, Biochimica et Biophysica Acta (BBA) -. General Subjects 2011;1810 (6):612–9.

[44] Ha YM, Kim J-A, Park YJ, Park D, Choi YJ, Kim JM, et al. Synthesis and biological activity of hydroxybenzylidenyl pyrrolidine-2,5-dione derivatives as new potent inhibitors of tyrosinase. MedChemComm 2011;2(6):542. https://doi.org/10.1039/c0md00234h.

[45] Chung KW, Park YJ, Choi YJ, Park MH, Ha YM, Uehara Y, et al. Evaluation of in vitro and in vivo anti-melanogenic activity of a newly synthesized strong tyrosinase inhibitor (E)-3-(2,4 dihydroxybenzylidene)pyrrolidine-2,5-dione (3-DBP). BBA 2012;1820(7):962–9.

[46] Ha YM, Park YJ, Kim J-A, Park D, Park JY, Lee HJ, et al. Design and synthesis of 5-(substituted benzylidene)thiazolidine-2,4-dione derivatives as novel tyrosinase inhibitors. Eur J Med Chem 2012;49:245–52.

[47] Bae SJ, Ha YM, Park YJ, Park JY, Song YM, Ha TK, et al. Design, synthesis, and evaluation of (E)-N-substituted benzylidene-aniline derivatives as tyrosinase inhibitors. Eur J Med Chem 2012;57:383–90.

[48] Kim SH, Ha YM, Moon KM, Choi YJ, Park YJ, Jeong HO, et al. Anti-melanogenic effect of (Z)-5-(2,4-dihydroxybenzylidene) thiazolidine-2,4-dione, a novel tyrosinase inhibitor. Arch Pharmacal Res 2013;36(10):1189–97.

[49] Ha YM, Lee HJ, Park D, Jeong HO, Park JY, Park YJ, et al. Molecular docking studies of (1E,3E,5E)-1,6-Bis(substituted phenyl)hexa-1,3,5-triene and 1,4-Bis (substituted trans-styryl)benzene analogs as novel tyrosinase inhibitors. Biol Pharm Bull 2013;36(1):55–65.

[50] Kim HR, Lee HJ, Choi YJ, Park YJ, Woo Y, Kim SJ, et al. Benzylidene-linked thiohydantoin derivatives as inhibitors of tyrosinase and melanogenesis: importance of the β-phenyl-α, β-unsaturated carbonyl functionality. MedChemComm 2014;5(9):1410–7.

[51] Son S, Kim H, Yun HY, Kim DH, Ullah S, Kim SJ, et al. (E)-2-Cyano-3-(substituted phenyl)acrylamide analogs as potent inhibitors of tyrosinase: A linear β-phenyl-α, β-unsaturated carbonyl scaffold. Bioorg Med Chem 2015;23 (24):7728–34.

[52] Kang KH, Lee B, Son S, Yun HY, Moon KM, Jeong HO, et al. (Z)-2-(Benzo[d] thiazol-2-ylamino)-5-(substituted benzylidene)thiazol-4(5H)-one Derivatives as Novel Tyrosinase Inhibitors. Biol Pharm Bull 2015;38(8):1227–33.

[53] Yun HY, Kim DH, Son S, Ullah S, Kim SJ, Kim YJ, et al. Design, synthesis, and anti-melanogenic effects of (E)-2-benzoyl-3-(substituted phenyl) acrylonitriles. Drug design, development and therapy 2015;9:4259–68.

[54] E.K. Lee, Kim, Ju Hyun, Moon, Kyoung Mi, Ha, Sugyeong, Noh, Sang-Gyun, Kim, Dae Hyun, Chung, Hae Young, ((E)-2-(substituted benzylidene)-2,3-dihydro-1H-cyclopenta[a]naphthalen-1-one derivatives inhibiting tyrosinase activity., Journal of the Life Sciences 27(2) (2017) 139-48.

[55] Lee B, Moon KM, Lim JS, Park Y, Kim DH, Son S, et al. 2-(3, 4-dihydroxybenzylidene)malononitrile as a novel anti-melanogenic compound. Oncotarget 2017;8(53):91481–93.

[56] H.J. Jung, M.J. Lee, Y.J. Park, S.G. Noh, A.K. Lee, K.M. Moon, E.K. Lee, E.J. Bang, Y.J. Park, S.J. Kim, J. Yang, S. Ullah, P. Chun, Y.S. Jung, H.R. Moon, H.Y. Chung, A novel synthetic compound, (Z)-5-(3-hydroxy-4-methoxybenzylidene)-2-iminothiazolidin-4-one (MHY773) inhibits mushroom tyrosinase, Bioscience, biotechnology, and biochemistry (2018) 1-9.

[57] Ullah S, Park Y, Ikram M, Lee S, Park C, Kang D, et al. Design, synthesis and anti-melanogenic effect of cinnamamide derivatives. Bioorg Med Chem 2018;26 (21):5672–81.

[58] H.J. Jung, A.K. Lee, Y.J. Park, S. Lee, D. Kang, Y.S. Jung, H.Y. Chung, H.R. Moon, (2E,5E)-2,5-Bis(3-hydroxy-4-methoxybenzylidene) cyclopentanone Exerts Anti-Melanogenesis and Anti-Wrinkle Activities in B16F10 Melanoma and Hs27 Fibroblast Cells, Molecules (Basel, Switzerland) 23(6) (2018) 1415.

[59] Kim CS, Noh SG, Park Y, Kang D, Chun P, Chung HY, et al. A Potent Tyrosinase Inhibitor, (E)-3-(2,4-Dihydroxyphenyl)-1-(thiophen-2-yl)prop-2-en-1-one, with Anti-Melanogenesis Properties in α-MSH and IBMX-Induced B16F10 Melanoma Cells, Molecules (Basel. Switzerland) 2018;23(10):2725.

[60] Ullah S, Park C, Ikram M, Kang D, Lee S, Yang J, et al. Tyrosinase inhibition and anti-melanin generation effect of cinnamamide analogues. Bioorg Chem 2019;87:43–55.

[61] Ullah S, Park Y, Park C, Lee S, Kang D, Yang J, et al. Antioxidant, anti-tyrosinase and anti-melanogenic effects of (E)-2,3-diphenylacrylic acid derivatives. Bioorg Med Chem 2019;27(11):2192–200.

[62] Lee S, Ullah S, Park C, Won Lee H, Kang D, Yang J, et al. Inhibitory effects of N-(acryloyl)benzamide derivatives on tyrosinase and melanogenesis. Bioorg Med Chem 2019;27(17):3929–37.

[63] Jung HJ, Noh SG, Park Y, Kang D, Chun P, Chung HY, et al. In vitro and in silico insights into tyrosinase inhibitors with (E)-benzylidene-1-indanone derivatives, Computational and Structural. Biotechnol J 2019;17:1255–64.

[64] Bang E, Lee EK, Noh SG, Jung HJ, Moon KM, Park MH, et al. In vitro and in vivo evidence of tyrosinase inhibitory activity of a synthesized (Z)-5-(3-hydroxy-4-methoxybenzylidene)-2-thioxothiazolidin-4-one (5-HMT). Exp Dermatol 2019;28(6):734–7.

[65] Ullah S, Kang D, Lee S, Ikram M, Park C, Park Y, et al. Synthesis of cinnamic amide derivatives and their anti-melanogenic effect in α-MSH-stimulated B16F10 melanoma cells. Eur J Med Chem 2019;161:78–92.

[66] Jung HJ, Noh SG, Ryu IY, Park C, Lee JY, Chun P, et al. (E)-1-(Furan-2-yl)-(substituted phenyl)prop-2-en-1-one Derivatives as Tyrosinase Inhibitors and Melanogenesis Inhibition: An In Vitro and In Silico Study. Molecules (Basel, Switzerland) 2020;25(22):5460.

[67] Chaudhari H, Pujari H. Heterocyclic systems containing bridge head nitrogen atom. i. synthesis of 5h 6h-imidazo-[2, ib]-thiazolidin-3-one hydrochloride. J Indian Chem Soc 1968;45(8):710-+.

[68] Urbano M, Guerrero M, Velaparthi S, Crisp M, Chase P, Hodder P, et al. Discovery, synthesis and SAR analysis of novel selective small molecule S1P4-R agonists based on a (2Z,5Z)-5-((pyrrol-3-yl)methylene)-3-alkyl-2-(alkylimino) thiazolidin-4-one chemotype. Bioorg Med Chem Lett 2011;21(22):6739–45.

[69] Bakbardina OV, Nurmagambetova RT, Gazalieva MA, Fazylov SD, Temreshev II. Synthesis and fungicidal activity of pseudo-thiohydantoins, their 5-arylidene derivatives, and 5-arylidene-3-β-aminothiazolid-2,4-one hydrochlorides. Pharm Chem J 2006;40(10):537–9.

[70] Vogeli U, Philipsborn WV, Nagarajan K, Nair MD. C-13-Nmr Spectroscopy. 19. Structures of Addition-Products of Acetylene-Dicarboxylic Acid-Esters with Various Dinucleophiles - Application of C, H-Spin-Coupling Constants. Helv Chim Acta 1978;61(2):607–17.

[71] VanAllan JA. 2-Carboxymethylmercaptobenzimidazole and Related Compounds*. J Org Chem 1956;21(1):24–7.

[72] Hyun SK, Lee W-H, Jeong DM, Kim Y, Choi JS. Inhibitory Effects of Kurarinol, Kuraridinol, and Trifolirhizin from <i>Sophora flavescens</i> on Tyrosinase and Melanin Synthesis. Biol Pharm Bull 2008;31(1):154–8.

[73] Ryu IY, Choi I, Jung HJ, Ullah S, Choi H, Al-Amin M, et al. In vitro anti-melanogenic effects of chimeric compounds, 2-(substituted benzylidene)-1,3-indanedione derivatives with a β-phenyl-α, β -unsaturated dicarbonyl scaffold. Bioorg Chem 2021;109:104688.

[74] Hassan M, Ashraf Z, Abbas Q, Raza H, Seo S-Y. Exploration of novel human tyrosinase inhibitors by molecular modeling, docking and simulation studies. Interdiscip Sci: Comput Life Sci 2018;10(1):68–80.

[75] Saeed A, Mahesar PA, Channar PA, Abbas Q, Larik FA, Hassan M, et al. Synthesis, molecular docking studies of coumarinyl-pyrazolinyl substituted thiazoles as non-competitive inhibitors of mushroom tyrosinase. Bioorg Chem 2017;74:187–96.

[76] Larik FA, Saeed A, Channar PA, Muqadar U, Abbas Q, Hassan M, et al. Design, synthesis, kinetic mechanism and molecular docking studies of novel 1-pentanoyl-3-arylthioureas as inhibitors of mushroom tyrosinase and free radical scavengers. Eur J Med Chem 2017;141:273–81.

[77] Friesner RA, Murphy RB, Repasky MP, Frye LL, Greenwood JR, Halgren TA, et al. Extra precision glide: Docking and scoring incorporating a model of hydrophobic enclosure for protein− ligand complexes. J Med Chem 2006;49 (21):6177–96.

[78] Farid R, Day T, Friesner RA, Pearlstein RA. New insights about HERG blockade obtained from protein modeling, potential energy mapping, and docking studies. Bioorg Med Chem 2006;14(9):3160–73.

[79] Kim H, Roh HS, Kim JE, Park SD, Park WH, Moon J-Y. Compound K attenuates stromal cell-derived growth factor 1 (SDF-1)-induced migration of C6 glioma cells. Nutr Res Pract 2016;10(3):259.

[80] Bae SJ, Ha YM, Kim J-A, Park JY, Ha TK, Park D, et al. A Novel Synthesized Tyrosinase Inhibitor: (E)-2-((2,4-Dihydroxyphenyl)diazenyl)phenyl 4-Methylbenzenesulfonate as an Azo-Resveratrol Analog. Biosci Biotechnol Biochem 2013;77(1):65–72.

[81] Chen L-G, Chang W-L, Lee C-J, Lee L-T, Shih C-M, Wang C-C. Melanogenesis Inhibition by Gallotannins from Chinese Galls in B16 Mouse Melanoma Cells. Biol Pharm Bull 2009;32(8):1447–52.